Modeling of an Electrochemical Flow-through Reactor for Mediated Alcohol Oxidation

M.L. Doorn

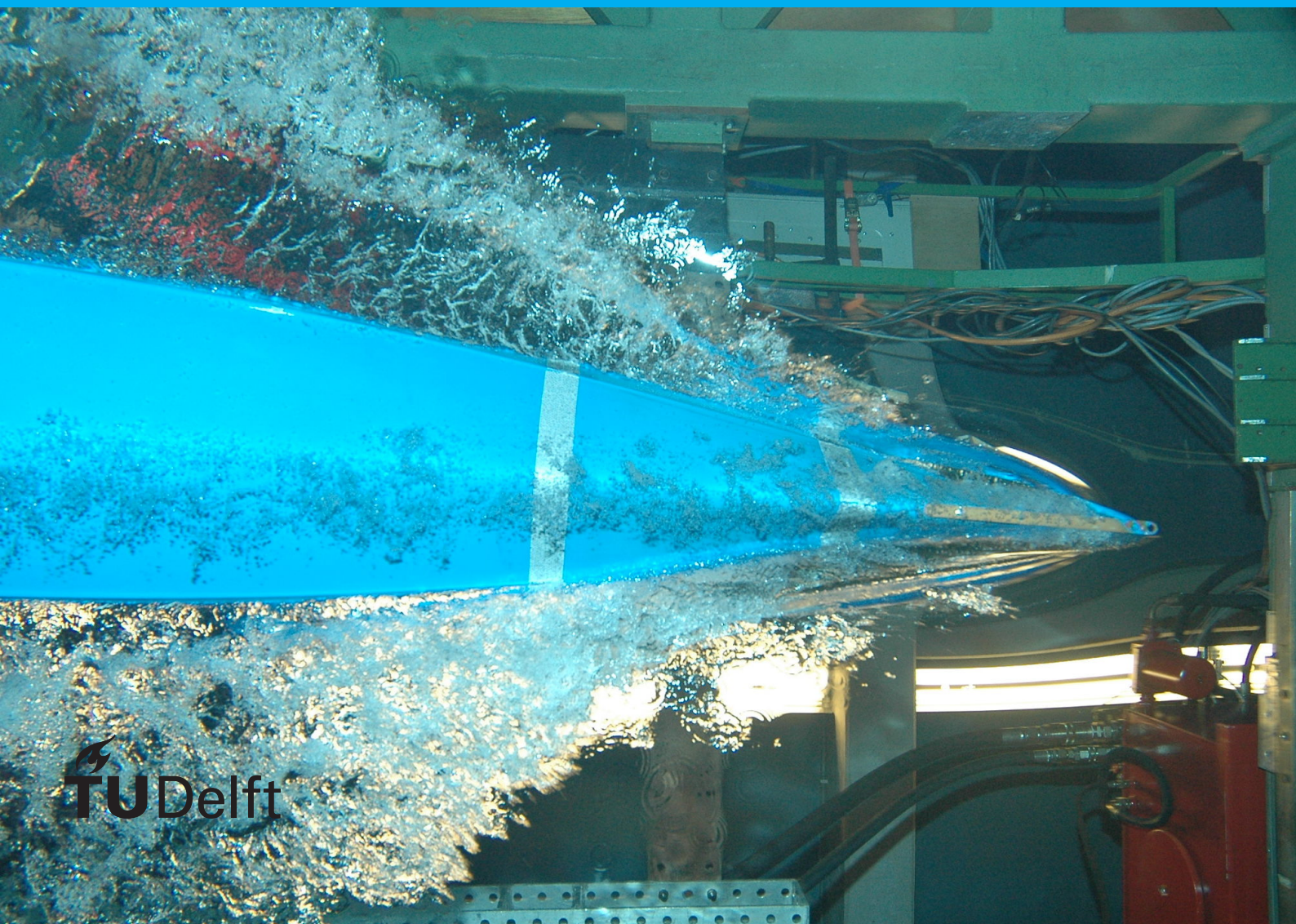

TU Delft

Modeling of an Electrochemical Flow-through Reactor for Mediated Alcohol Oxidation

by

M.L. Doorn

to obtain the degree of Master of Science
at the Delft University of Technology,
to be defended publicly on Thursday August 13, 2020 at 10:00 AM.

Student number:	4310284	
Project duration:	August 1, 2019 – August 13, 2020	
Thesis committee:	Dr. ir. J.W. Haverkort,	TU Delft, supervisor
	Prof. dr. ir. E.L.V. Goetheer,	TU Delft, Chair
	Dr. ir. T.E. Burdyny,	TU Delft
	Dr. ir. R. Latsuzbaia,	TNO

TU Delft

Acknowledgement

My research is incomplete without thanking the people who have played a key role in the creation of this work. First, I would like to express my gratitude towards Willem Haverkort for his support, contributions and above all for his patience. Willem's contagious enthusiasm for the subject matter motivated me to not shy away from any challenges.

Secondly, I would like to express my appreciation towards Roman Latsuzbaia, for his guidance throughout my research. He has been there to support me every step of the way. Roman, thank you for the great *chemistry*.

Lastly, I would like to thank TNO SPES for facilitating my research. It was a very special and educational experience. A special thanks to Saskia Bubberman who has helped me with performing the experiments needed for this report.

Max Doorn
August, 2020

Abstract

The increasing penetration of renewable energy in the energy grid causes intermittency, resulting in fluctuating prices. This in turn forges windows of opportunity for the electrochemical production of chemicals that would otherwise be too expensive. This research aims to optimize a continuous-flow-through reactor hosting the production of chemicals by mediated electrochemical oxidation, using organic aminoxyls (i.e., electrocatalysts), specifically 2,2,6,6-tetramethylpiperidinyloxyl (TEMPO) and 4-acetamido-TEMPO (ACT).

The first chapter addresses the main motivation behind- and the aims of the this research. In the second chapter, an extensive literature review is provided on the physico-chemical and electro-catalytic properties of the TEMPO mediators, that are important for the modelling of the electrochemical reactor. The third chapter describes the analytical- and computational models that were created to investigate the influence of mediator properties, current density, specific surface area, velocity, and electrode thickness on the energy efficiency of the reactor. More specifically, a flow-through electrochemical reactor with metal foam electrodes and divided anolyte and catholyte compartments.

The solutions obtained from the analytical model are in good agreement with the solutions of the computational model. The analytical model was extended with the Hatta analysis to include mass transfer in the porous electrode. It was found that ohmic losses, due to an expanding reaction zone from the membrane inward in the anode, caused by mass-transfer and/or kinetic limitations of the mediator, pose the biggest obstacle in reaching high conversion with reasonable efficiency.

The main result of this study is a mathematical formula, that allows for quick prediction of the performance of mediated electrochemical oxidation in a flow-through reactor with a porous foam electrode.

Contents

Nomenclature

Physics Constants

b	Tafel slope	0.05 V
F	Faraday constant	96485 C mol^{-1}
R	Gas constant	8.314 J mol^{-1} K^{-1}

Roman Symbols

ΔV	total overpotential with the activation potetial as reference	V
A	Area	m^2
a_v	Volumetric surface area	m^2 m-3
B	Pre-exponential factor Arrhenius equation	L mol^{-1}
c	Concentration of oxidezed mediator unless told differently	mol m^{-3}
D	Diffusivity	m^2 s^{-1}
d_{eq}	Equivalent diameter 6/a_v	m
E	Potential	V
E_a	Activation potential	V
f	Friction factor	-
I	Current	A
i	Current Density	A m^{-2}
j	Current density	C s^{-1} m^{-1}
J_a	Activation energy	kJ mol^{-1}
j_{**}	Exchange current density	A m^{-2}
K	Permeability	m^2
k	Homogeneous rate constant	s^{-1}
k_0	Heterogeneous rate constant	m s^{-1}
K_B	Buffer equilibrium constant	-
k_b	Backward rate constant	s^{-1}
k_f	Forward rate constant	m^3 s^{-1} mol^{-1}
k_m	Mass transfer coefficient	m s^{-1}
K_W	Water equilibrium constant	-
L	Electrode thickness	m
l	Shortest path length in porous medium	m

N	Flux of a species	mol m^{-2} s^{-1}
n	Number of electrons participating in the reaction	-
P	Power	W
p	Pressure	N m^{-2}
r	rare of the reaction	mol m^{-3} s^{-1}
T	Temperature	K
x	Coordinate in the electrode	m
z	Number of elementary charges	–
ρ_e	Charge density	C m^{-3}
h	Cell height	m
R	Resistance	Ω
r	Rate of reaction	mol $s^{-1} m^{-3}$
w	Cell width	m

Greek Symbols

δ	Boundary layer thickness	m
$\mathcal{E}$	Effectiveness factor	-
ρ	Density	kg m^{-3}
θ	Enhancement factor	-
α	Charge transfer coefficient	-
δ	Boundary layer thickness	m
ϵ	Porosity	-
η	Activation overpotential	V
ϵ	Ratio of void volume over the total volume	-
κ	ionic conductivity	Ω^{-1} m^{-1}
μ	Dynamic viscousity	kg m^{-1} s^{-1}
Φ	Potential	V
ρ	Density	kg m^{-3}
σ	Conductivity of the electrolyte	Ω^{-1} m^{-1}
τ	Toruosity	-

Dimensionless numbers

$\overline{\eta}$	Normalized activation overpotential	$\eta\, b^{-1}$
$\overline{c}$	Normalized concentration of oxidezed mediator unless told differently	$c\, c_0^{-1}$
$\overline{i}$	Ratio of current density in the electrode vs the total current density	$i_{e^-}(x)\, i_x^{-1}$
$\overline{j}_*$	Current normalized by the total superficial exchange current density	$j\, (k_0\, F\, c_0\, L\, a_v)^{-1}$

$\bar{j}_{\kappa}$	Inverse Wagner number for the electrolyte	$j\,L\,b^{-1}\,\kappa^{-1}$
$\bar{j}_{\sigma}$	Inverse Wagner number for the electrode	$j\,L\,b^{-1}\,\sigma^{-1}$
$\bar{j}_{m}$	Current Normalized by the maximum achievable current due tomass transfer	$j(N_m\,F\,L\,a_v)^{-1}$
$\bar{j}_{\kappa+\sigma}$	Inverse Wagner number for the parallel resistance	
j_r	Current normalized by the maximum current density achievable by chemical reaction	$j\,(k\,c_0\,F\,L\,\epsilon)^{-1}$
M_T	Thiele modulus	$L_p\sqrt{k/D}^{-1}$
AL	Hinterland ratio	$\epsilon k_m a_v^{-1} D^{-1}$
Ha	Hatta number	$\sqrt{kD}\;k_m^{-1}$
Re	Reynolds number	$u\,L\,\rho\,\mu^{-1}$
Sc	Schmidt number	$\mu\,\rho^{-1}\,D^{-1}$

Abbreviations

ACT	4-acetamido-TEMPO
CV	cyclic voltammetry
LA	lactic acid
PDO	1,2-propandiol
TEMPO	2,2,6,6-tetramethylpiperidinyloxyl

Superscripts

0	Indicating the formal potential
$brugg$	Bruggman factor

Subscripts

0	Initial or membrane coordinate
eq	Equilibrium
i	Species
o	Oxidant
r	Reductant
V	Constant Volume
buff	Concerning the buffer
e^-	Electronic
ion^-	Ionic
lim	Limiting current density
loc	Local
s	Solid

1

Introduction

Renewable energy sources account for an ever-increasing share of the total energy generation. One of the main challenges of renewable energy sources, such as solar and wind, is intermittency: when the sun is shining and the wind is blowing, there is an abundance of electricity, but on a windless night, no energy is produced. Since prices fluctuate with demand and supply, cheap energy is available at days of abundance. This cheap electricity improves the business case for the electrochemical production of chemicals, as they usually require significant energy input to facilitate chemical conversion.

1.1. Background

Electrochemical production of chemicals is a process in which electricity is used to transform various molecules into target chemicals, of which the most basic process is water electrolysis, shown in Figure 1.1 [42].

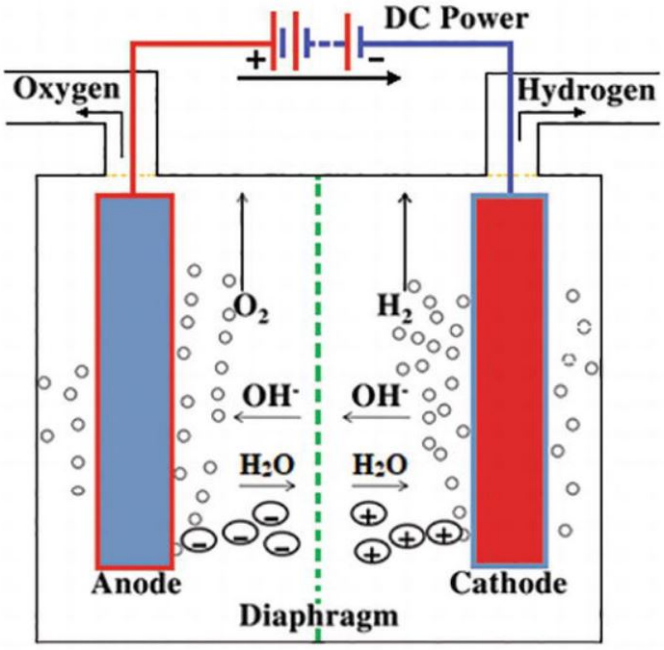

Figure 1.1: Alkaline water electrolysis, extracted from [42]

During water electrolysis, the current from the DC power source applied to an electrochemical reactor

supplies electrons to the cathode, where water is split into hydrogen and hydroxide ion. The hydrogen leaves the compartment as a gas, while the hydroxide ions move in the electrolyte through the diaphragm, towards an anode. On the anode, the electron is transferred back into the electric circuit, and the hydroxide ions form water and oxygen. Therefore, a reduction reaction takes place on the cathode and oxidation on the anode. However, if oxygen is not produced under high pressure, it is of a little economic value. Pairing the cathodic process with a different anodic process, in which a value-added chemical is produced, could yield a sound business case. This is already done with chlor-alkali electrolysis [20], where chlorine is produced at the anode.

TNO is developing a process in which 1,2-propanediol, a chemical which can be easily produced from bio-based glycerol, by-product in the production of bio-diesel [46], is turned into lactic acid. The latter is used for the production of polylactic acid (PLA) of which as Lunt describes: ”The basic properties lie between those of crystal polystyrene and PET” [41]. However, instead of a direct electrochemical oxidation as shown in Figure 1.1, a mediated electrochemical oxidation is used to transform propandiol into lactic acid.

During a mediated electrochemical oxidation, a redox mediator molecule is oxidized on an anode, after which an oxidized form of the mediator diffuses away from the electrode surface and oxidizes a reactant into a target molecule in the bulk of the electrolyte. Then, the reduced form of the mediator is transformed back into the original oxidation state and the process is repeated. This way the mediator is continuously recycled. The mediated oxidation of propandiol to lactic acid is shown on Figure 1.2. In this process the organic aminoxyl (i.e.,electrocatalysts) TEMPO, is oxidized into TEMPO+ which is an active oxidant for propandiol oxidation to lactic acid in the bulk of the electrolyte.

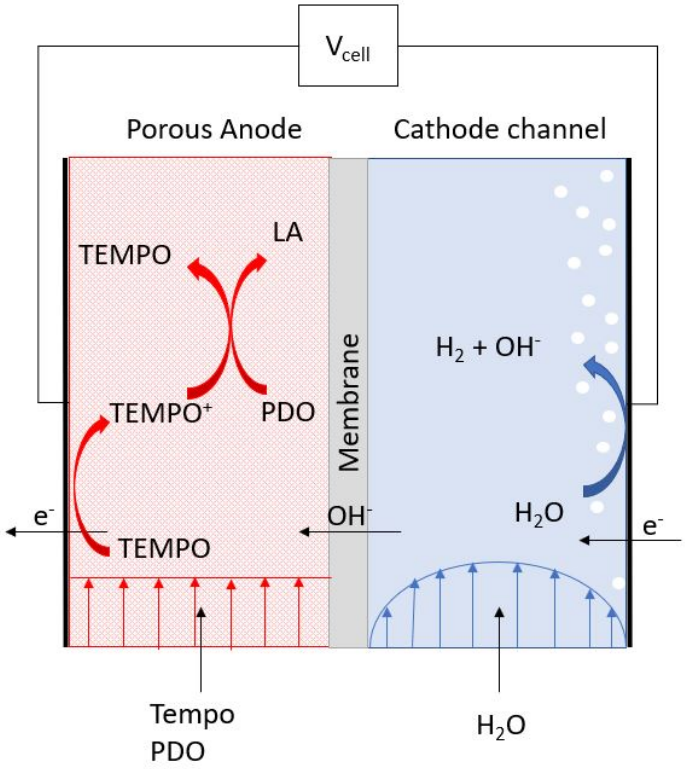

Figure 1.2: At the cathode, the reduction of water into hydrogen and hydroxide ion is portrayed. Hydrogen leaves the cathode compartment at the top and the hydroxide, and travels through the membrane towards the anode. At the anode, first TEMPO is oxidized at the electrode surface, to $TEMPO^+$, after which it oxidizes propandiol into lactic acid by reducing itself back into TEMPO.

The main motivation to use TEMPO mediated propandiol oxidation is the reduced cost, since affordable, porous electrode materials can be used for TEMPO activation. This is interesting, since direct electro-

chemical oxidation of PDO is typically performed using gold or platinum, which is rather expensive. [11]

When pairing electrochemical processes, they must have compatible achievable current densities, i.e. the limiting currents. Physical phenomena, mostly mass transfer, cause this limitation. We know that the reduction of water is done at high current densities. However, the mediated oxidation of propanediol is researched by TNO [47], and the current density in a flow-by configuration reached a maximum of 35 [mA/cm ^{2}]. The main issue was the mass transfer of the mediator from and to the bulk. In order to increase the mass transfer, a pulsation in the electrolyte flow was introduced and this resulted in an increased current density of 45 [mA/cm ^{2}].

This thesis looks into an alternative way to increase anode current density, via a design of a reactor utilizing porous anode, which will effectively increase the specific surface area, which in turn increases the current density to a level that is compatible with the water reduction.

1.2. Research Questions

- Which chemical characteristics of organic aminoxyl mediators are determining for the speed of conversion in a flow through reactor?
- How do current density, volumetric surface area, velocity and electrode thickness influence the efficiency of a flow-through reactor with a porous foam electrode?

1.3. Approach

In order to answer the first research question, an extensive review will be made of the available literature on the mediator and its interaction with the propanediol.

In order to answer the second research question regarding the influence of geometrical and condition parameters on the efficiency of the cell, two models will be created: an analytical and a 2D computational model. Both models will be based on a lab-scale, continuous flow reactor, allowing for efficient validation of the models.

There are many electrochemical models available already, such as the analytical model from Haverkort [29], and a 2D model from Shah [53], the latter focusing on a liquid flow battery. Models with a coupled electrochemical and chemical reaction are more scarce however. Scott did design such a model for a packed-bed reactor [52]. However, neither of the models mentioned above make use of a mediator. In Do's 1D model [19] a mediator was used, however it was immobilized in a catalytic layer.

The model envisioned for this research is one incorporating activation, ohmic, and mass transfer losses together with frictional losses for mediated oxidation in a porous electrode. To the best of the author's knowledge, no such model exists.

2

Theory

This chapter provides a theoretical overview that forms the basis of this research. Firstly, electrochemical reactions, mechanisms, and kinetics are elucidated. Secondly, bulk chemical reactions are covered. Finally, mass transport and hydrodynamics are discussed.

2.1. Electrochemistry

This section will first focus on the equations governing the electron transfer from and to the electrode. Second, it will discuss the current distribution, followed by an extensive review of TEMPO mediated oxidation of 1,2-propanediol.

2.1.1. Kinetics

Butler-Volmer

"Experience demonstrates that the potential of an electrode strongly affects the rate of reactions occurring on its surface" [5]. The Butler-Volmer equation provides an intuitive explanation for this phenomenon. The equation "or a variation derived from it, is used in the treatment of almost every problem requiring an account of heterogeneous kinetics" [5]. The Butler-Volmer equation used in this work also allows one to quantify the overpotential losses due to mass transport limitations resulting in the concentration dependent Butler-Volmer:

$$j = nFk_0\left(c_o e^{\left[\frac{\alpha F}{RT}(E-E^0)\right]} - c_r e^{-\left[\frac{(1-\alpha)F}{RT}(E-E^0)\right]}\right), \tag{2.1}$$

where, j is the current density,n the amount of electrons transferred, F the Faraday constant, α is the symmetry factor, also referred to as the charge transfer coefficient, E is the potential, E^0 is the standard potential, c_o is the concentration of oxidized species, c_r is the concentration of the reduced species and k_0 standard rate constant.

Tafel

In the exponents of equation 2.1 is the term $(E - E_0)$ is referred to as overpotential η. At high overpotentials, the right term of equation 2.1 goes to zero, making it negligible. With this assumption of a high overpotential the Butler-Volmer formulation reduces to the Tafel equation:

$$\eta = b \ln\left(\frac{j}{j_{**}}\right). \tag{2.2}$$

where, the exchange current density is defined as: $j_{**} = k_0 F c_{eq}$ and $\frac{RT}{\alpha F}$ is referred to as b, also known as the Tafel slope.

2.1.2. Current Distribution

General Conductivity

Generally the relationship between current flowing through a conductor and voltage is described by Ohm's law 3.6. which introduces the resistance as a ratio between the two. In electrochemisty Ohm's law is still very applicable only resistance is described differently. Pouillet's law 2.4 is used to describe the resistance based on a materials conductivity, cross-sectional area and its length. combining the two gives the equation 2.5:

$$R = \frac{E}{I}, \tag{2.3}$$

$$R = \frac{L}{A\kappa}, \tag{2.4}$$

$$\phi_{\text{ion}^-} = \frac{IL}{A\kappa} = \frac{jL}{\kappa}, \quad \phi_{\text{e}^-} = \frac{jL}{\sigma}, \tag{2.5}$$

where R is the resistance in $[\Omega]$, i is the current in $[A]$, A is the area in [m^2], ϕ_{ion^-} and ϕ_{e^-} are the ohmic potential losses in the electrolyte and electrode respectively in [V], j is the current density [A m^{-2}], L is the length the current has to travel in [m], and κ is the conductivity of the the electrolyte in [Ω^{-1}m^{-1}] and σ is the conductivity of the electrode in [Ω^{-1}m^{-1}].

Electrolyte

In order to minimize ohmic losses in an electrochemical reactor, an electrolyte with sufficient ionic conductivity is required. For this purpose, inorganic supporting electrolytes of inert salts, acids, and bases are used. Since supporting electrolytes do not participate in the reactions, and are present in large quantities compared to the reacting ions, the conductivity can be assumed to be constant [43]. This research uses a buffer solution to ensure a constant pH and it simultaneously acts as a supporting electrolyte. The working of the buffer is further elaborated upon in section 2.2.2. The ohmic loss in the electrolyte obeys Equation 2.5, where κ the conventional symbol for conductivity in the liquid phase. The electrolyte conductivity, depends on the characteristics of the buffer and its concentration.

Electrode

The electrode is also subjected to Ohm's law, equation 2.5, σ is used, the conventional symbol for conductivity in the solid phase. Conductivity is usually given as a material property, here σ_s. However, in a porous electrode, the conductivity is not only a material property but also a geometrical property.

Since only part of the electrode volume is filled with the solid material, σ_m, needs to be multiplied by $(1-\epsilon)$. Secondly, most porous media are chaotic, foams used in this research are no exception. Foams consist of small ligaments attached to one another, forming a chaotic network of wires. These wires expand in all directions, only the wires in the x-direction, normal to the current collector, will contribute to the conductivity. Therefore, the σ_s needs to be divided by 3, giving the following modified equation, established by Lemlich [39] , for the electrode conductivity:

$$\sigma = \frac{1}{3}(1-\epsilon)\sigma_s. \tag{2.6}$$

Despite its simplicity, it shows strong resemblance to experiments with high porosity open-cell foams, as acknowledged by [26] [13].

2.1.3. Electrochemical Thiele Modulus

The Thiele Modulus originates from the chemical industry [54] and is used to calculate the effectiveness of catalytic particles in chemical reactors. It does so "... by comparing the actual mean reaction rate within the pore with the rate if not slowed by pore diffusion" [40], as depicted in equation 2.7. For this derivation a slender pore inside a catalytic particle is considered, as shown in Figure 2.1 extracted from [40].

$$\mathcal{E} = \frac{\text{actual mean reaction rate within pore}}{\text{rate if not slowed by pore diffusion}} = \frac{\langle c \rangle}{c_0}, \tag{2.7}$$

this can be equated since the rate is proportional to the concentration of the reactant. For determining

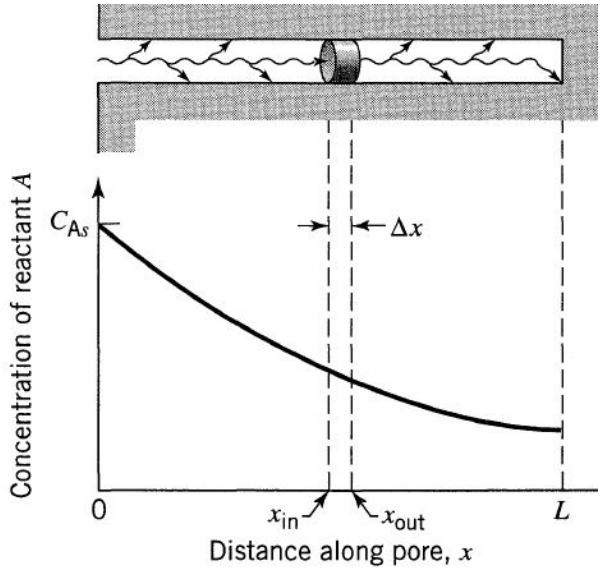

Figure 2.1: At the top is a schematic representation of a slender pore in a catalytic particle. The graph, underneath the schematic, plots the concentration of reactant A. It shows that at the inlet of the pore the concentration is the highest. Moving inside the pore the concentration will drop. The figure was extracted from [40]

the average concentration the Thiele modulus is introduced and used to find the pore effectiveness, derived in [40]:

$$\mathcal{E} = \frac{\langle c \rangle}{c_0} = \frac{\tanh(M_T)}{M_T} \quad \text{where, } M_T = \frac{L_p}{\sqrt{k/D}}, \tag{2.8}$$

from this function follows that when $M_T < 0.4$ the effectiveness becomes $\mathcal{E} \approx 1$ and when $M_T > 4$, $\mathcal{E} = \frac{1}{M_T}$.

Haverkort introduced an electrode effectiveness factor for porous electrodes [29]. Similar to the chemical effectiveness, again the average reaction rate is compared with the maximum reaction rate. However, here the rate is expressed in current. Following the Tafel equation the current is determined by the amount of activation overpotential, η. This implies that the place with the maximum current is located where the overpotential is highest, which is at the membrane, as indicated in Figure 2.2.

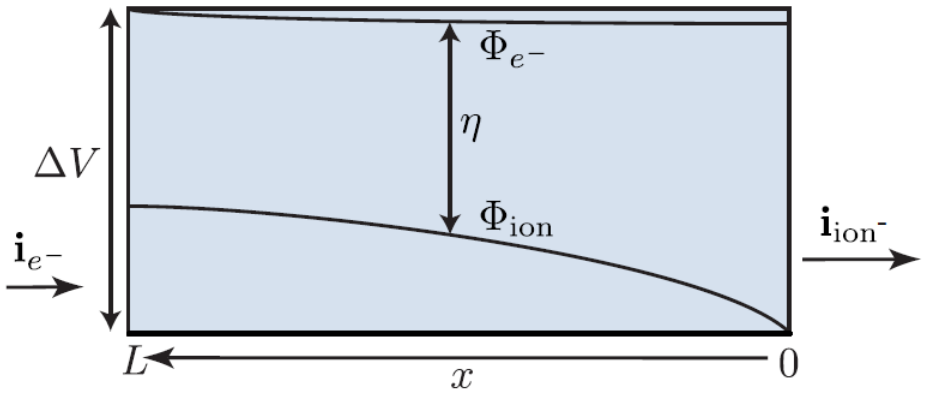

Figure 2.2: Schematic of the porous electrode. x is defined as zero at the membrane and 1 at the current collector. ϕ_{e^-}, indicates the potential in the electrode, ϕ_{ion^-} the potential in the electrolyte, $\mathbf{i}_{e^-}$ is the electronic current, $\mathbf{i}_{\text{ion}^-}$ is the ionic current and ΔV is the total overpotential of the half cell. The figure was extracted from [29].

Similar to the effectiveness factor of equation 2.8, the average rate is compared with the maximum

rate to determine the electrode's effectiveness:

$$\mathcal{E} = \frac{\langle j' \rangle}{j_0'} = \frac{j}{j_0'} = \frac{1}{\bar{j}_0'} = \frac{\bar{j}_*}{e^{\overline{\eta}_0}}, \tag{2.9}$$

where:

$$\bar{j}_* = \frac{j}{j_*}, \text{ where } j_* = k_0 F c_0 L a_v, \tag{2.10}$$

and $\overline{\eta} = \eta / b$. Also a_v is the volumetric surface area and L the electrode thickness. Rewriting equation 2.9 yields:

$$\overline{\eta}_0 = \ln\left(\frac{\bar{j}_*}{\mathcal{E}}\right), \tag{2.11}$$

here $\mathcal{E}$ can again be described by $\tanh(M)/M$, where M is a modulus which can be dependent on transport limitations or ohmic losses inside the electrode.

2.1.4. TEMPO Mediated Electrochemcial Oxidation

Electrochemical alcohol oxidation methods using organic aminoxyl mediators (i.e., electrocatalysts) have advanced considerably in recent years, and they provide a compelling alternative to the more traditional chemical methods [45]. The mediated oxidation methods are appealing, in part, because they generate hydrogen gas as the sole byproduct of the reaction on the cathode side[50]. Next to that, these aminoxyl mediators can be oxidized on inert materials such as carbon electrodes eliminating the need for noble metals as electrode material. In this section, the mechanism of mediated oxidation, by such a organic aminoxyl mediator; 2,2,6,6-Tetramethylpiperidine-1-oxyl (TEMPO) will be discussed. Moreover, TEMPO will be compared to its derivative 4-acetamido-TEMPO (ACT) and the parameters influencing this oxidation reaction will be identified. TEMPO, schematically represented in Figure 2.3a, was first electrochemically investigated by Tsunaga et al. in 1973 [55]. By analyzing cyclic voltammograms (CV), they found that TEMPO was chemically reversible. Meaning that the "... electron transfer between the electrode and the analyte is fast on the time scale of mass transfer" [35]. This reversibility is also maintained in aqueous solutions.

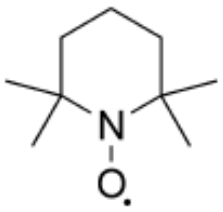

(a) schematic of TEMPO

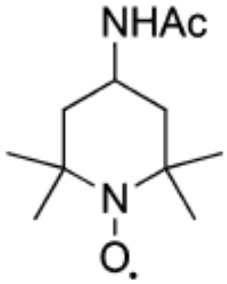

(b) schematic of ACT

To date, there are over 100 of TEMPO derivatives synthesized and studied [31]. In this research, only TEMPO and ACT are considered. The reason for including ACT was, Raffie [50] found, that: "the low-cost aminoxyl, ACT was found to be a highly effective mediator for electrocatalytic oxidation of various simple alcohols." Furthermore, they demonstrated the preparative-scale utility of ACT-mediated oxidation of primary alcohols and aldehydes to carboxylic acids.

The molecular structures of ACT and TEMPO are very similar, with the difference that ACT has an additional acetamido group, schematically represented in Figure 2.3b. Despite their similar molecular structures, their catalytic performance, activation potential, and diffusion coefficients differ. As displayed in Figure 2.6, where two CV's are depicted, CV is a powerful and popular electrochemical technique commonly employed to investigate the redox properties of molecular species[22].

Before comparing TEMPO and ACT, it is key to understand how organc aminoxyl mediators work. First the more common, non-oxidized, version of TEMPO as shown in Figure 2.3a, is oxidized at the electrode into $TEMPO^+$. Thereafter, $TEMPO^+$ is reduced by an alcohol into TEMPOH. The oxidation of the alcohol is graphically demonstrated in Figure 2.4 extracted from [48].

The combination of an alcohol-to-aldehyde reaction and an aldehyde-to-acid reaction results in a 2 electron/2 proton reaction. TEMPO does this by forming an adduct with alcohol or aldehyde. First, the oxygen in the primary alcohol group, of the alcohol, bounds with the nitrogen in TEMPO, essentially kicking out a proton. Thereafter, this proton is injected into the electrolyte. Next, a proton from the

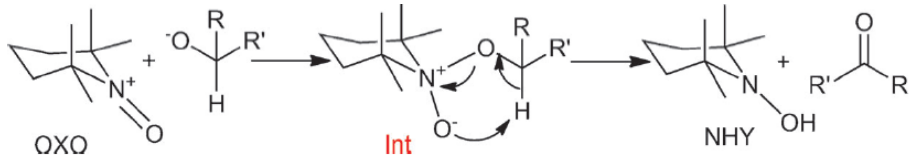

Figure 2.4: Proposed mechanism for the oxidation of alcohols by TEMPO under basic conditions [48].

carbon atom to which the the primary alcohol was attached bounds with the oxygen on TEMPO. This leaves the alcohol with a double oxygen bound instead of an OH group and TEMPO is converted to TEMPOH.

What happens next is still under debate, there are two options in the literature: first, the TEMPOH is oxidized at the electrode with a two electron transfer and the proton is released into the electrolyte. Second, TEMPOH reacts with $TEMPO^+$ forming two TEMPO molecules and the then oxidizes again to $TEMPO^+$ at the electrode, this is called *comprotonisation*. The process is shown in Figure 2.5 extracted from Nutting [45].

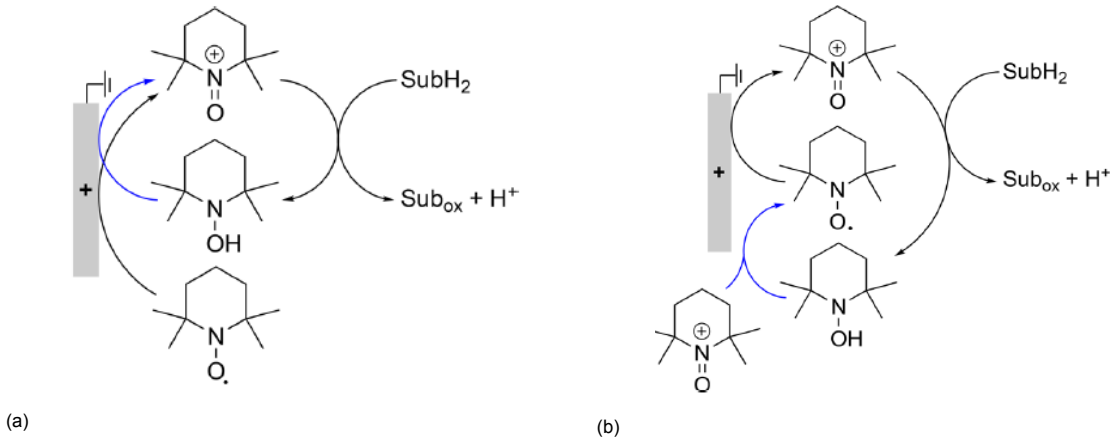

(a) (b)

Figure 2.5: Possible mechanisms for regeneration of $TEMPO^+$ in electrocatalytic reactions, (a) direct electron transfer and (b) comprotonisation. Extracted form [45].

However, the conclusion drawn by Israeli et al. is that the comprotonisation with a rate constant of 52 [M^{-1} s^{-1}] is not fast enough to contribute toward the recycling of TEMPO [33]. Therefore, in this work, the mechanism shown in Figure 2.5a will be used. Hickey et al. [31] proved that this mechanism consists of two reactions: first, the oxidation of TEMPO to $TEMPO^+$ and the second, the oxidation of TEMPOH to TEMPO involving a proton. However, this second reaction happens at a lower potential and is thus not limiting, depending on the pH.

$$\mathrm{TEMPO} \longrightarrow \mathrm{TEMPO}^+ + \mathrm{e}^- \tag{2.12}$$

$$\mathrm{TEMPOH} + \mathrm{OH}^- \longrightarrow \mathrm{TEMPO} + \mathrm{H_2O} + \mathrm{e}^- \tag{2.13}$$

Now there is a basic understanding of how TEMPO and ACT work. Figure 2.6 shows how TEMPO and ACT compare, this is done with cyclic voltammetry (CV) measurements, a powerful and popular electrochemical technique commonly employed to investigate the redox properties of molecular species [22]. They were conducted in both the absence and presence of 1,2-propanediol (PDO). Figure 2.6a shows a CV of TEMPO and ACT in absence of PDO. Here both TEMPO and ACT have their peak anode/cathode potentials close to each other, indicating reversibility. The current of TEMPO starts to rise earlier than ACT showing that TEMPO has a lower activation potential. Also, the peak current of TEMPO is higher compared to ACT, which suggests TEMPO has a better diffusivity. In Figure 2.6b one finds the CV with PDO added to the solution. With both TEMPO and ACT, the cathodic peak decreased, and the anodic peak increased. The decrease in cathodic peak current is caused by the reaction between the substrate, here PDO, and the mediator reduces the mediator. So after the reaction, there

is no oxidized mediator left to reduce, therefore, no peak. The increase in anodic peak current is due to the mediator's regeneration, resulting in a higher concentration of unoxidized mediator available close to the electrode. The speed of regeneration is determined by the rate of the reaction between the mediator and the substrate. When TEMPO and ACT are compared, ACT achieves a higher anodic peak current, translating to a higher reaction rate, between ACT and the substrate compared to TEMPO.

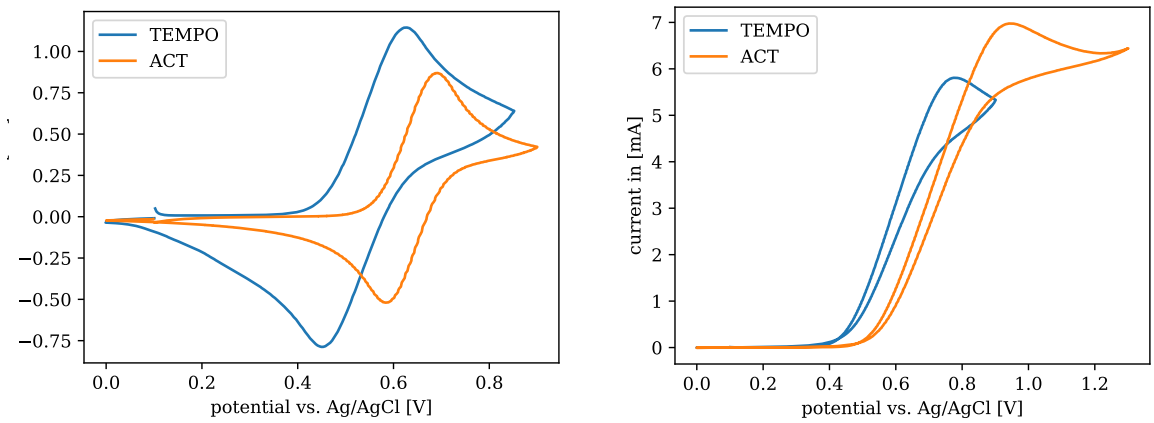

Figure 2.6: (a) Cyclic voltametry of 15 mM TEMPO and 15 mM ACT with a scan rate of 10 mVs in an aqueous solution with a 0.5 M borate buffer at pH 9.2, (b) with 140 mM of PDO added. The experiments were conducted during this work, appendix A describes how they were executed.

As to why ACT is more catalytically active than TEMPO, literature was consulted. Hickey et al. provided the following explanation: "The catalytic activity is directly proportional to the inverse of the oxidation potentials E_{a1} and E_{a2}" [31], where E_{a1} belongs to reaction 2.13 and E_{a2} to reaction 2.12. However, by their theory, TEMPO should be more catalytically active then ACT, which is contradicted by Raffie et al.[49]. Raffie argues the enhanced performance is due to the higher driving force given by ACT's higher potential compared to TEMPO. Therefore, at this moment, no univocal conclusions can be drawn from the existing literature about why ACT is more catalytically active than TEMPO.

One conclusion that can be drawn however, is that an elevated pH enhances the catalytic performance. This can be seen in Figure 2.7, extracted form Raffie's work [48]. In which CV's are shown of TEMPO both in the absence and presence of a substrate and at different pH values. The figure 2.7 indicates that at an elevated pH the reaction rate of the chemical reaction increases:

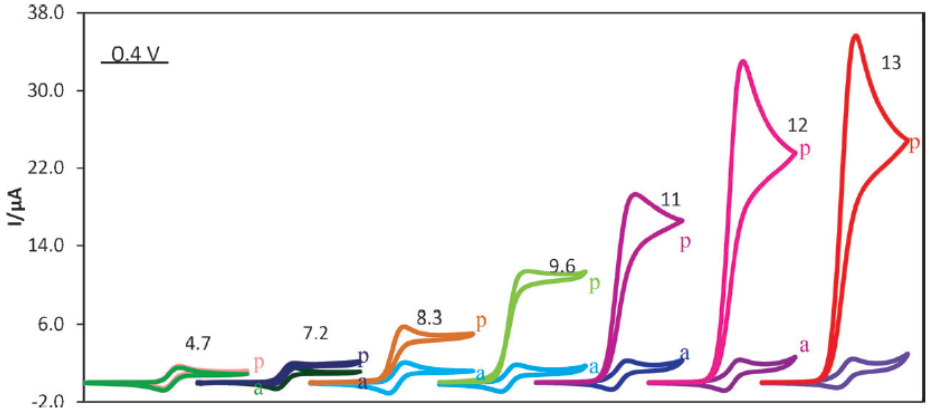

Figure 2.7: CVs of 10 mM TEMPO in the absence (a) and presence of 10 mM BA (p) in buffer solution at various pH values. Scan rate: 10 mV/s, extracted form [48].

This could be due to the steric effect argued by Raffie [48] or by the decrease in potential 2.13 argued by Hickey et al. [31]. Either way, pH is an key parameter in determining the conditions inside

the reactor; not only because of the enhanced performance but also to ensure stability of TEMPO or ACT, as pointed out by Stahl et al. [24], who made Pourbaix diagrams of both TEMPO and ACT, presented in Figure 2.8.

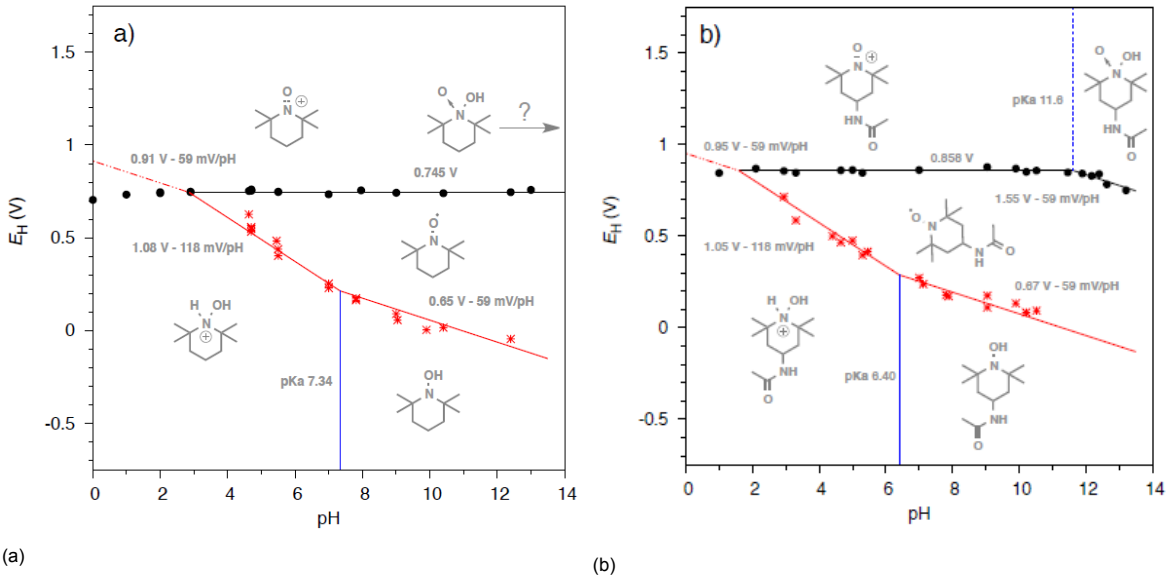

(a) (b)

Figure 2.8: Pourbaix diagrams of TEMPO (a) and ACT (b). Extracted from [24].

Figure 2.8a shows that if the pH drops below 7 when TEMPO gets reduced, it will reduce to $TEMPH_2^+$, which is an electrochemically inactive species and can only be chemically oxidized again by $TEMPO^+$. However, this process is slow. Thus, when the pH drops below 7, TEMPO will be reduced to an electrochemically inactive species and thereby ending its cyclic oxidation of alcohol. For ACT, this happens around pH 6.4.

The same issue arises at an elevated pH, although not visible in Figure 2.8a. In 2.8b, it becomes clear that at a pH of 11.8 or higher, ACT is transformed to ACT-OH. This molecule is electrochemically inactive as well, causing the cyclic oxidation to be crippled.

This phenomenon is incredibly important when designing a reactor. For ACT, this means that the pH cannot drop below a pH of 6.4 and not exceed a pH of 11.8, which is challenging considering that four hydroxides ions are used to convert one PDO ion into LA and two for LA to PA. A buffer is needed, to keep the reaction working as it is supposed to.

Summary and Properties

Based on the literature review this will be the parameters used for the design and modeling of a reactor, the following aspects from the previous section will be considered. First the oxidation reaction; the oxidation of TEMPOH is viewed as two steps, where the last step, TEMPO to TEMPO+, is the limiting step; therefore, the only electrochemical reaction modeled.

Secondly, the reactor's pH should stay between 7 and 14 for TEMPO and 6.4 and 11.8 for ACT.

TEMPO Properties							
	D 10^{10} [m^2/s]	E_α [V]	E_{eq}[V]	k_0 10^4 [m/s]	method	pH	T [°C]
Stalh [24]	7.5		0.745		CV	3-14	n/a
Glandut[25]	7.7				CV, sim	n/a	n/a
Fish [23]	51		0.731	3.10E-05	CV, anlysis	2-12	n/a
Janiszewska [34]	5.52		0.708	1.50E-04	CV, RDE, sim	7	25
Hickey [31][30]	12.34	0.53	0.74		CV,sim	7,	25
This work	6.36				CV	9.2	20
This work	3.25			2.33E-04	RDE	9.2	20

Table 2.1: Chemical properties of TEMPO

ACT properties							
	D 10^{10} [m^2/s]	E_α [V]	E_{eq}[V]	k_0 10^4 [m/s]	method	pH	T [°C]
Stalh [24]			0.858		CV	2-11.6	n/a
Hickey [31]		0.635			CV,sim	7	25
This work	3.53			1.97E-04	RDE	9.2	20
This work	3.22				CV	9.2	20

Table 2.2: Chemical properties of ACT

2.2. Chemical Reactions

The previous section explained how the electrochemical alcohol oxidation using organic aminoxyl mediators works. This section discusses what reaction path is taken in converting 1,2-propanediol (PDO) to Lactic acid (LA), what the limiting step in this process is, and what at what rate this step proceeds. The oxidation of PDO is already covered in a couple of papers [11][18]. with the reaction paths displayed in in Figure 2.9 form Chadderdon et al. [11]. However, in these papers, PDO was directly oxidized on gold and platinum electrodes, whereas this research intends to use a mediator as a chemical catalyst.

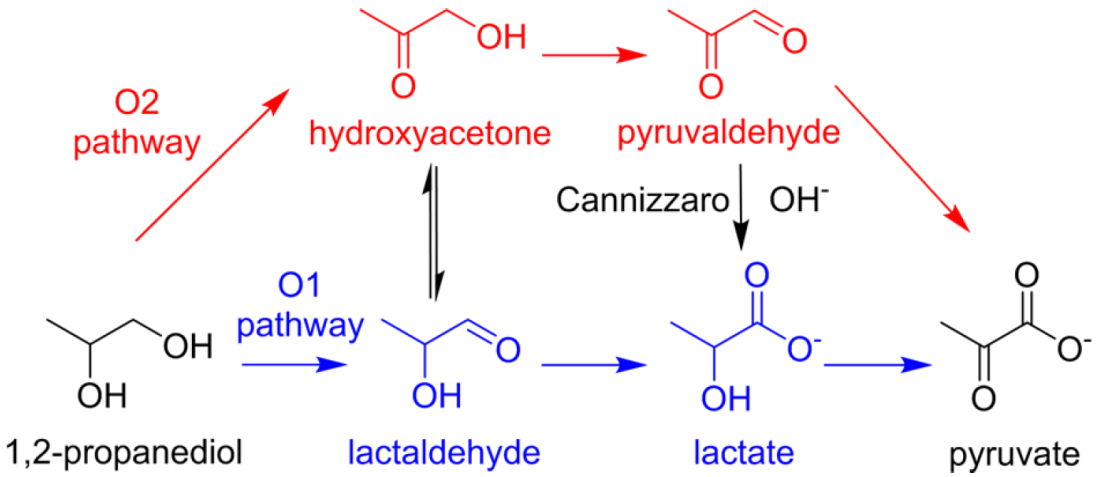

Figure 2.9: Reaction paths form propandiol to pyruvate, note that Lactate is the substance of interest. Extracted from [11]

.

2.2.1. The Coupled Reaction

Path

A good understanding of the reaction mechanism of the conversion of PDO into LA is needed to ensure an adequate model solution. Generally, the fastest way to get from molecule A to molecule B is the reaction path. In this reaction-chain, the slowest link is the rate-determining step. Hickey et al. performed research on the mediated oxidation of glycerol to CO2 with TEMPO, where each step of the process was measured separately with a CV. This study provides insight into the slower and faster steps in the process, as shown in Figure 2.10: Although glycerol and PDO are not the same, they are similar. Therefore, it is assumed that the steps proceed with the same relative rate to each other. The oxidation of the aldehyde (molecule 2 in Figure 2.10) shows the highest conversion. Second is the oxidation of glycerol itself. Aldehyde is found in both paths. However, if the aldehyde in the second path were to be oxidized, it would end up as pyruvate. This together with the findings of Raffie et al. [48], who say TEMPO and it is derivatives are catalytically more active towards primary alcohols compared to secondary alcohols, makes pathway O1 as displayed in Figure 2.9 the most likely.

Rate

The combination of PDO with TEMPO or ACT is not reviewed in literature. Therefore, a way had to be found to get these rate constants. Numerous CV's and RDE experiments where conducted to achieve

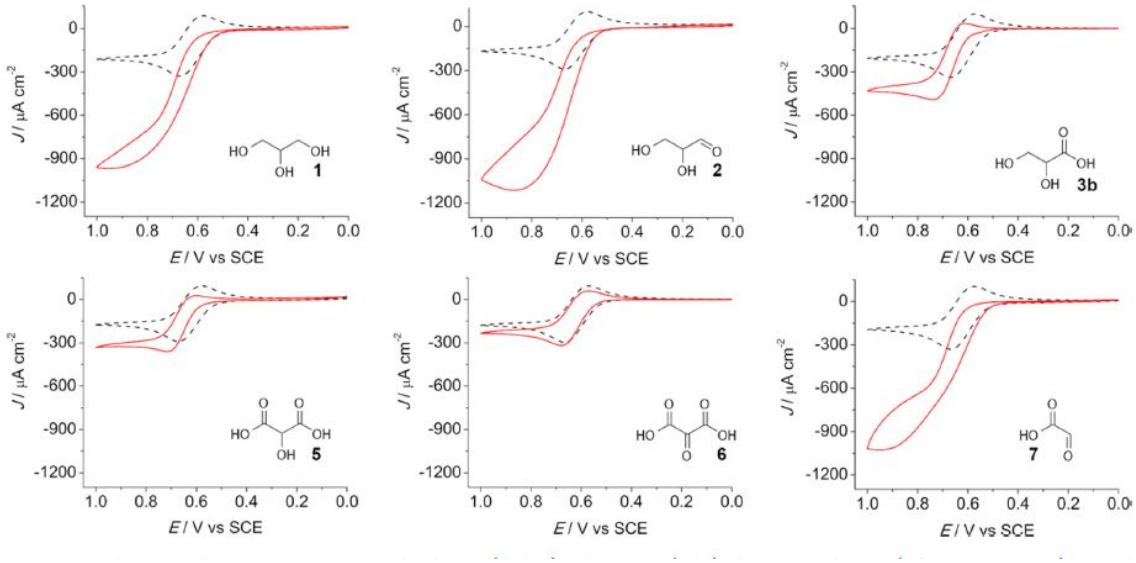

Figure 2.10: CV's of the oxidation steps from glycerol towards CO_2 with a schematic of the oxidized molecule displayed in each CV. Extracted form [30]

.

this. These experiments together with analytical tools such as a foot-of-wave-analysis [12][37][38], fitting CV's with a CV model in COMSOL, and other methods as described in [44] and [51], are supposed to give a value for the rate of the reaction. In the end, Lee et al. [37], suggested a way to extract a rate constant for the oxidation of PDO by ACT from an CV experiment. How this is done is covered in appendix A. The experiments also displayed that at elevated concentrations of the PDO, the concentration of the substrate had no influence on the rate. The influence of pH on the rate is not taken into account in this research, since the solution is buffered at a constant pH. Leading to a first order rate equation:

$$r = k[A], \tag{2.14}$$

where k is the rate constant in [1/s], [A] is the concentration of rate-determining species [mol m^{-3}] and r is the rate of the reaction in [mol m^{-3} s^{-1}]

Chemical reaction	k [1/s]	rate equation
PDO + 2 $TEMPO^+$ + 2 OH^- $\longrightarrow$ LA + 2 TEMPOOH + 2 H_2O	1.9	r = k [$TEMPO^+$]
PDO + 2 ACT^+ + 2 OH^- $\longrightarrow$ LA + 2 ACTH + 2 H_2O	5.5	r = k [$TEMPO^+$]

Table 2.3: The chemical reactions considered with there rate and rate equation.

2.2.2. The Buffer

A buffer is used to keep a solution or goods at a stable pH. pH is defined as:

$$\text{pH} = -\log[\text{H}^+] \tag{2.15}$$

So in order to have this "buffering" effect, the concentration of protons [H^+] has to be maintained. This is done by adding a weak acid; AH, and its conjugate base; A^-, to a solution obtaining the following equation:

$$\text{AH} \rightleftharpoons \text{H}^+ + \text{A}^- \tag{2.16}$$

One can see when acid is added to a buffered solution, the equilibrium of equation 2.16 shifts towards the right-hand side and the concentration of [H^+] goes back to its original value, hence the solution is buffered. The value of pH is determined by the equilibrium constant of equation 2.16.

The Anodic compartment is buffered at a pH of 9.2, which is in the stable region of both TEMPO and ACT: Figure 2.8b. For this report, a borate buffer was used, which is cheap and widely available(source).

The borate buffer consists of boric acid H_3BO_3, acting as weak acid, and tetrahydroxyborate H_4BO_4, acting as the conjugate base, resulting in the following reaction:

$$H_3BO_3 + OH^- \rightleftharpoons H_4BO_4{}^- \tag{2.17}$$

Note that equation 2.17 is written with OH^- instead of H^+ because this is more convenient since OH^- is used in the reaction to form LA. The equilibrium constant is kPa $= 9.14$, which can be expressed as:

$$K_B = \frac{[H_3BO_3][OH^-]}{[H_4BO_4{}^-]} = -\log_{10}(9.14) \tag{2.18}$$

Where K_B is the equilibrium constant of the boric acid buffer. For modeling purposes it is key know how fast balance is restored when the equilibrium is disturbed. R. E. Zeebe and D. Wolf-Gladrow [16] investigated this buffer and came up with the following expressions for the forward and backward rate constants, using the Arrhenius equation for the forward rate constant:

$$k_f = Be^{\frac{-J_a}{RT}}, \tag{2.19}$$

where, the pre-exponetial factor; B = $4.58\ 10^{10}$ L mol^{-1}, the activation energy; $J_a = 20.8$ kJ mol^{-1}, this results in a forward rate constant of;f $k_f = 1.04\ 10^{-7}$ L mol^{-1} s^{-1}. For the backward rate constant they used the following expression:

$$k_b = \frac{k_f}{K_B} = k_f \frac{K_W}{K_B}, \tag{2.20}$$

where, K_W is the equilibrium constant for water and backward rate constant, $k_b = 256$ s^{-1} for water at 25 °C.

Buffer reaction	pK_{eq}	k_f [m^3/(s mol)]	k_b [1/s]
$H_3BO_3 + OH^- \rightleftharpoons H_4BO_4{}^-$	9.14	9005.43	124.30

Table 2.4: Equilibrium constants of the buffer.

2.3. Mass Transport

This section focuses on the mass transport in the Porous electrode. There are three ways of mass transportation in a porous electrode; Advection, Migration, and Diffusion. Migration is the mass transport of ions in an electrolyte driven by the electric-field (potential). However, since a buffer is used, which acts as a supporting electrolyte, Migration is negligible [60]. Leaving only Advection and Diffusion.

There are also two ways to look at mass transfer, or as put by Boomsma: ”Modeling of porous media flows of the nature we are interested in falls under two distinct categories: macroscopic, where volume averaging is performed and microscopic, where the details of the flow in/around individual structural elements of the medium are examined” [9]. In this work, all analyses are done on the macroscopic scale: First a general overview of the hydrodynamics and diffusion in porous media, then the mass transfer of the buffer to the membrane and finally the mass transfer from the electrode surface to the bulk.

2.3.1. Porous Electrode

Porous electrodes enhance the surface area on which an electrochemical reaction can take place but it also impacts the mass-transport. This section establishes the vocabulary needed to describe the mass transport in porous media.

Tortuosity (τ) expresses the fact that the length of the microscopic level flow, or transport, through the actual(microscopic) tortuous pathways within the void-space is larger than the length of averaged transport [7].:

$$\tau = \frac{l_{||}}{l}, \tag{2.21}$$

where, $l_{||}$ is the actual path traveled by the molecule and l is the shortest path.

Bruggeman correlation empirically Bruggeman found that:

$$\tau \approx \frac{1}{\sqrt{\epsilon}}. \tag{2.22}$$

Equivalent diameter (d_{eq}) is an approximation of the pore size in porous media. Equation 2.23 gives this estimation for a solid foam [7]:

$$d_{eq} = \frac{6}{a_v}, \tag{2.23}$$

where a_v is the volumetric surface area.

2.3.2. Diffusion

The superficial species flux $N_{i,x}$ in [mol m^{-2}s^{-1}] can be calculated using Fick's law:

$$N_i = -D_e \frac{dc}{dx}, \tag{2.24}$$

where D_e is the effective diffusivity, which can be calculated as follows:

$$D_e = D\frac{\epsilon}{\tau} \approx D\epsilon^{brugg}, \tag{2.25}$$

where, D is the molecular diffusivity commonly used in Fick's law, $brugg$ is the Bruggman factor which is normally around 1.5.

2.3.3. Continuity

In the porous electrode mass is preserved leading to the following equation for continuity:

$$\epsilon\frac{\partial \rho}{\partial t} + \nabla \cdot (\rho \mathbf{v}) = 0, \tag{2.26}$$

where **v** the velocity vector is volume averaged [21], meaning that velocity deviations in the pores are averaged out. With a plug flow, the velocity is taken constant over the whole porous medium,

The reason for this difference, compared with, Hagen-Poussuille, where the velocity is a function of position, is that over the volume of a porous electrode, the surface area causes friction between the fluid and the solid, is equally distributed. Whereas with Hagen-Poussuille, there is only friction on the side walls. Locally in the pores, there are velocity differences, but when looking at the whole electrode, they are averaged out.

2.3.4. Buffer Depletion at the Membrane

The advantage of porous electrodes is the extra surface area aiming to increasing the current density. In order to facilitate high current densities, big ionic fluxes are required between the electrodes. Since the ion-carrying species is hydroxide, see Figure 1.2, an increase in pH at the membrane can be expected. Even when the solution is buffered it is questionable whether the buffer can hold the pH steady. This can be problematic because, as mentioned in section 3.1.3, when the pH exceeds a certain level the mediator stops working. In [6] an estimate is derived to quantify the maximum flux to a wall in a plug-flow, which is the same problem encountered here.

$$j_{\text{lim}} = \frac{F c_{\text{buff}} \sqrt{u D_{\text{buff}}}}{\sqrt{h}}, \tag{2.27}$$

where j_{lim} is the limiting current imposed by the buffer, c_{buff} the concentration of the buffering species of the buffer, u is the superficial velocity and D_{buff} is the diffusion coefficient of the buffer.

2.3.5. Mass Transport in the Pores

For most of this research, perfect mixing in the pores is assumed. Meaning the concentration in the pore is the same as the electrode surface. However, this is somewhat paradoxical, to get a species from the wall into the pore mass transfer is needed. The driving force for mass transfer is the concentration gradient. So in order to have perfect mixing, concentration gradients are required.

In fact there are stagnant boundary layers [4], which determine the mass transport between the surface and the bulk. In literature this is referred to as external mass transfer, Bracconi at al.[10] state that the performance of open-cell foams is ”limited by external heat and mass transfer”. To quantify the amount of mass transfer, mass transfer coefficients (k_m) are used, which can by calculated with equation 2.28. Where the Sherwood number, Sh is a correlation based on the structure of the medium and the flow through or past it. In literature there are two Sherwood correlations for open-cell foams, such as used in this research, found in table 2.5.

$$k_m = \frac{\mathrm{Sh}D}{d_{eq}}. \tag{2.28}$$

soucre	Range	Formula
Das [4]	$\mathrm{Re} > 10$	$\mathrm{Sh} = 1.94 + 0.41\mathrm{Re}^{0.52}\mathrm{Sc}^{0.33}$
Bracconi [10]	$1 < \mathrm{Re} < 100$	$\mathrm{Sh}_{d_{s,avg}} = \epsilon^{-2}(0.566\mathrm{Re}_{d_{s,avg}}^{0.33} + 0.0039\mathrm{Re}_{d_{s,avg}}^{0.8})\mathrm{Sc}^{1/3}$

Table 2.5: Sherwood numbers for opencell foams found in literature

However, the fact that during this mass transfer the species transported is also reacting complicates the matter. This brings us to the Hatta number which ”compares the rate of reaction in a liquid film to the rate of diffusion through the film.”[8] and is provided in equation 2.29. The Hatta analysis introduced in 1932 [27], was originally applied to reactors with a liquid gas interface, where the gas dissolves into the liquid phase where it reacts [56] [57]. In such reactors a stagnant layer would develop between the bulk and the gas/liquid interface. The Hatta analysis allows one to calculate what the yield of the reactor would be.

The problem described above in the gas/liquid reactor is very similar to the problem presented in this report. The difference is that instead of a gas/liquid interface there is a solid/liquid interface. The condition of a constant concentration is still maintained because of the regeneration of the mediator. It is not the first time it is used in combination with electrochemistry [52].

$$\mathrm{Ha} = \delta_m\sqrt{\frac{k}{D}} = \frac{\sqrt{kD}}{k_m}, \tag{2.29}$$

where δ_m is the mass transfer boundary layer. The Hatta number can then be used to calculate the maximum flux form the wall of the reacting species, in this case the oxidized mediator, shown in equation 2.30, extracted from [57].

$$N_m = \frac{D}{\delta}c_0\mathrm{Ha}\frac{\mathrm{Ha}(\mathrm{AL}-1) + \tanh(\mathrm{Ha})}{\mathrm{Ha}(\mathrm{AL}-1)\tanh(\mathrm{Ha}) + 1}, \tag{2.30}$$

here N_m is the maximum flux achievable by the mass transfer, AL is the Hinterland ratio AL is defined as the ratio between the total reaction phase volume and the reaction phase film volume [56], given in equation 2.31:

$$\mathrm{AL} = \frac{\epsilon}{a_v\delta_m} = \frac{\epsilon k_m}{a_v D} \tag{2.31}$$

If the following conditions are met: AL $\gg$ 1 and (AL-1) $\mathrm{Ha}^2 \gg 1$. equation 2.30 can be simplified into 2.33, using the the enhancement factor calculated in equation 2.32. This simplification provides an enhancement factor. This enhancement factor predicts the extra flux due to the chemical reaction in the boundary layer.

$$\Theta = \frac{\mathrm{Ha}}{\tanh(\mathrm{Ha})} \tag{2.32}$$

$$N_m = k_m \Delta c \Theta \tag{2.33}$$

Where, Δc_{med} would be the concentration difference between the wall and the bulk, the driving force. It is assumed, the concentration at the wall to be c_0. Figure 2.11 gives a schematic representation of the mass-transfer of the mediator between the bulk and the electrode surface. With the dashed line indicating the concentration profile without reaction in the boundary layer and the solid line indicating the concentration profile with the reaction taken into account. In addition to equation 2.33 an expression

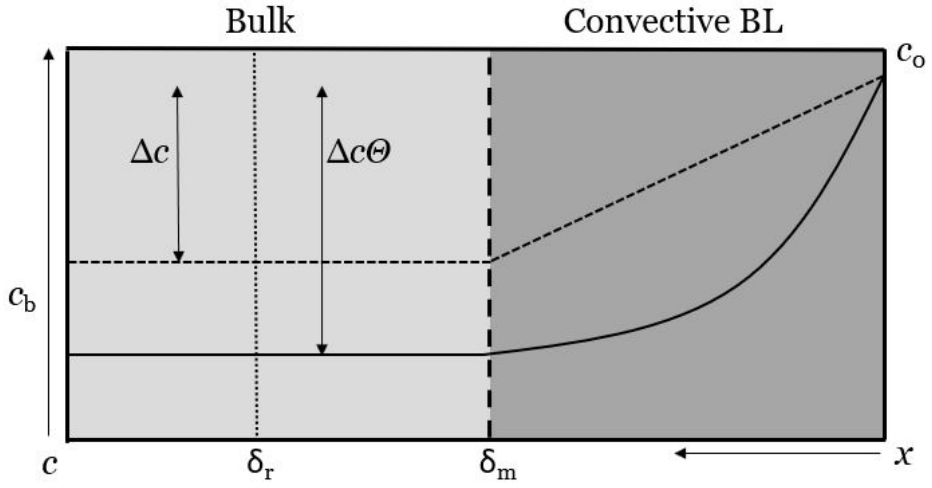

Figure 2.11: A schematic of the concentration profile of the mediator between electrode surface at $x = 0$ to the bulk at $x = \delta_m$, the mass-transfer boundary thickness. The dashed line indicates the profile without reaction and the solid line indicates the concentration profile with the reaction taken into account. The difference in bulk concentration presents the additional driving force of the flux yielding a higher mass-transfer.

for Δc_{med} can be found. Since the enhancement happens prior to the reaction in the bulk, with the assumption of steady state, the mass transfer and the reaction can be equated, in order to not use the boundary layer double ϵ was multiplied by (1-$\frac{1}{AL}$):

$$k c_b \epsilon (1 - \frac{1}{\text{AL}}) = k_m \Delta c \Theta a_v \tag{2.34}$$

resulting in an expression for the bulk concentration:

$$c_b = \frac{a_v \Theta k_m c_0}{a_v \Theta k_m + k\epsilon(1 - \frac{1}{\text{AL}})} \tag{2.35}$$

Leading to an equation for the maximum flux:

$$N_m = k_m \Theta c_0 \left(1 - \frac{a_v \Theta k_m}{a_v \Theta k_m + k\epsilon(1 - \frac{1}{\text{AL}})}\right) \tag{2.36}$$

3

Modeling

3.1. Analytical Model

The analytical model is an essential part of this report. It will indicate what might be the potential for an electrochemical mediated oxidation process with a few calculations. The mass transfer, activation potential, and ohmic losses are captured in one formula, which will be derived in section 3.1.3. Firstly however, this section elaborates on the assumptions that are made in creating the model and the hydrodynamics.

3.1.1. Assumptions

In order to create a comprehensive and insightful model, several assumptions were made:

- The reactor is in steady state;
- The electrode conductivity is a log bigger than the electrolyte conductivity $\sigma \gg \kappa$;
- Throughout the domain there is a constant ionic conductivity;
- Only the anode is considered, not the cathode;
- The chemical reaction of PDO to LA is a first order reaction dependent on the mediator concentration;
- pH stays stable throughout the electrode;
- No in- and outlet effects.
- Faradaic losses are not considered.

3.1.2. Hydrodynamics

Since the hydrodynamics inside a porous medium are complex, the most common way to model them is by using a correlation. The first one to make such a correlation was Darcy, whose equation was meant for slow moving fluids in soils, since he was a civil engineer. Later Ergun, a chemical engineer came up with a correlation for packed bed reactors, which as Das [15] puts it: ”For engineering purposes, the most well-known formula for predicting the pressure drop in a randomly packed-bed of particles is the Ergun correlation.” Although packed-beds consist of small spherical particles, which is different form a open-cell structure, they are similar. Therefore, in literature there are two correlations found based on the Ergun equation meant for open-cell foams.

$$\frac{\Delta p}{L} = \frac{f \mu u}{d_{eq}^2}, \tag{3.1}$$

different relations for the friction factor, presented in table 3.1

Source	Range	formula
Das [15]	Re > 20	$f_1 = 70.54\frac{(1-\epsilon)^{1.38}}{\epsilon^{4.5}} + 0.84\frac{(1-\epsilon)^{0.59}}{\epsilon^{3.11}} Re^{0.39+1.46\epsilon^{0.06}(1-\epsilon)^{0.51}}$
	20 <Re < 550	$f_2 = 70.54\frac{(1-\epsilon)^{1.38}}{\epsilon^{4.5}} + 1.95\frac{(1-\epsilon)^{1.18}}{\epsilon^{4.39}} Re$
Dietrich [17]	10^{-1} <Re< 10^5	$f = 247.5\frac{(1-\epsilon)^2}{\epsilon^3} + 2.175\frac{(1-\epsilon)}{\epsilon^3} Re$

Table 3.1: Friction factors for open-cell foams found in literature.

3.1.3. Electrochemistry

The analysis performed here is very similar to the one in [29]. The difference here is the extra reaction term of the chemical reaction in the bulk-solution. In order to make the analytical model more insightful, dimensionless numbers are used:

$$\bar{j}_r = \frac{j}{j_r}, \text{ where } j_r = kc_0FL\epsilon, \tag{3.2}$$

where j_r indicates the highest achievable current by the chemical reaction. Which is calculated by the highest possible reaction rate multiplied by the total void volume. Following equation 3.2 the maximum rate is achieved when all of the mediator is oxidized, yielding a concentration equal to the initial mediator concentration.

$$\bar{j}_* = \frac{j}{j_*}, \text{ where } j_* = k_0Fc_0La_v, \tag{3.3}$$

which is the current compared to the exchange current density. More normalized numbers are used in addition to the latter, to keep the derivation more readable:

$$\overline{\eta} = \frac{\eta}{b}, \quad \overline{c} = \frac{c}{c_0}, \quad \overline{x} = \frac{x}{L}, \quad \bar{i} = \frac{i_{e^-}(x)}{i_x}, \quad \bar{j}_\kappa = \frac{jL}{b\kappa}, \quad \bar{j}_\sigma = \frac{jL}{b\sigma}$$

Where the first is the normalized overpotential, the second is the concentration of the oxidized mediator normalized with the initial concentration of the mediator, the third is the current density in the electrode at a certain position and the fourth and fifth are the inverse Wagner numbers for the electrolyte and electrode respectfully. Finally, the inverse Wagner number for the parallel resistance is:

$$\bar{j}_{\kappa+\sigma} = \frac{jL}{b(\sigma+\kappa)}. \tag{3.4}$$

Tafel Kinetics

The analysis in this and the following sections closely follows that of [28]. Since the reactor is in steady state, the current used in the electrochemical reaction is the same as the amount of electrons needed for the chemical reaction. This can be explained because the two are linked in series therefore, the chemistry and the electrochemistry can be equated. For the electrochemisty Tafel is assumed, and there are no mass transport limitations.

$$\bar{i}' = \frac{\overline{c}}{\bar{j}_r} = \frac{(1-\overline{c})e^{\overline{\eta}}}{\bar{j}_*} = \frac{\bar{j}_*^{-1}e^{\overline{\eta}}}{1+\frac{\bar{j}_r}{\bar{j}_*}e^{\overline{\eta}}}, \tag{3.5}$$

where $\bar{i}$ is the ratio of the current density in the electrode over the total current density at a certain position, $\overline{c}$ is the normalized concentration of oxidized mediator, so $1-\overline{c}$ is the normalized concentration of unoxidized mediator, since $c_{\text{med},0} = c_{\text{med}} + c^+_{\text{med}}$. Note that the concentration is eliminated here. The result is put into Ohm's law, with the assumption that $\sigma \gg \kappa$ [29]:

$$\overline{\eta}' = \bar{j}_\kappa(\bar{i}-1), \tag{3.6}$$

filling equation 3.5 in 3.6 gives the following double derivative of the potential in the electrode:

$$\overline{\eta}'' = \frac{\bar{j}_\kappa}{\bar{j}_*} \frac{e^{\overline{\eta}}}{1 + \frac{\bar{j}_r}{\bar{j}_*} e^{\overline{\eta}}}, \tag{3.7}$$

by using the following relationship formulated in equation 3.8 for the left hand side, derived with the product rule and the chain rule: $\frac{d}{d\bar{x}} = \frac{d\overline{\eta}}{d\bar{x}} \frac{d}{d\overline{\eta}}$:

$$\overline{\eta}'' = \frac{d}{d\bar{x}}\left(\frac{d\overline{\eta}}{d\bar{x}}\right) = \frac{d\overline{\eta}}{d\bar{x}} \frac{d}{d\overline{\eta}}\left(\frac{d\overline{\eta}}{d\bar{x}}\right) = \overline{\eta}' \frac{d\overline{\eta}'}{d\overline{\eta}} = \frac{1}{2} \frac{d\overline{\eta}'^2}{d\overline{\eta}}. \tag{3.8}$$

Integrating equation 3.7 with using equation 3.8 gives:

$$\frac{\bar{j}_*}{2\bar{j}_\kappa}(\overline{\eta}_1'^2 - \overline{\eta}_0'^2) = \frac{\ln\left(1 + \frac{\bar{j}_r}{\bar{j}_*} e^{\overline{\eta}_1}\right) - \ln\left(1 + \frac{\bar{j}_r}{\bar{j}_*} e^{\overline{\eta}_0}\right)}{\frac{\bar{j}_r}{\bar{j}_*}} \tag{3.9}$$

Next is assumed that the exponent of the overpotential is considerably higher at the membrane compared to the current collector, meaning that $e^{\overline{\eta}_0} \gg e^{\overline{\eta}_1}$, thus $\ln\left(1 + \frac{\bar{j}_r}{\bar{j}_*} e^{\overline{\eta}_1}\right)$ is neglected. In addition, the derivative of $\overline{\eta}_1' = 0$ and $\overline{\eta}_0' = -\bar{j}_\kappa$, which leaves the following equation:

$$\frac{\bar{j}_r \bar{j}_\kappa}{2} = \ln\left(1 + \frac{\bar{j}_r}{\bar{j}_*} e^{\overline{\eta}_0}\right) \tag{3.10}$$

Resulting in an expression for $\overline{\eta}_0$:

$$\overline{\eta}_0 = \ln\left(\frac{e^{\frac{\bar{j}_\kappa \bar{j}_r}{2}} - 1}{\frac{\bar{j}_r}{\bar{j}_*}}\right) \tag{3.11}$$

This can then be used for the electrochemical Thiele Modulus, described in 2.1.3, just like in [29]:

$$\Delta\overline{V} = \ln\left(\frac{\bar{j}_*}{\mathcal{E}}\right) + \bar{j}_{\kappa+\sigma}, \text{ where } \mathcal{E} \approx \frac{1}{M}, \tag{3.12}$$

since $M \gg 1$. Leading to a electrode effectiveness described similar to the Thiele effectiveness:

$$\mathcal{E} = \frac{\tanh(M)}{M}, \quad \text{with, } M = \frac{e^{\frac{\bar{j}_\kappa \bar{j}_r}{2}} - 1}{\bar{j}_r} \tag{3.13}$$

At higher current densities, $e^{\frac{\bar{j}_\kappa \bar{j}_r}{2}} \gg 1$, which allows to simplify equation 3.12 to equation 3.14:

$$\Delta\overline{V} = \ln\left(\frac{\bar{j}_*}{\bar{j}_r}\right) + \frac{\bar{j}_\kappa \bar{j}_r}{2} \tag{3.14}$$

Which can be rewritten into dimensional quantities:

$$\Delta V = b \ln\left(\frac{k\epsilon}{k_0 a_v}\right) + \frac{j^2}{2kc_0\epsilon\kappa} \tag{3.15}$$

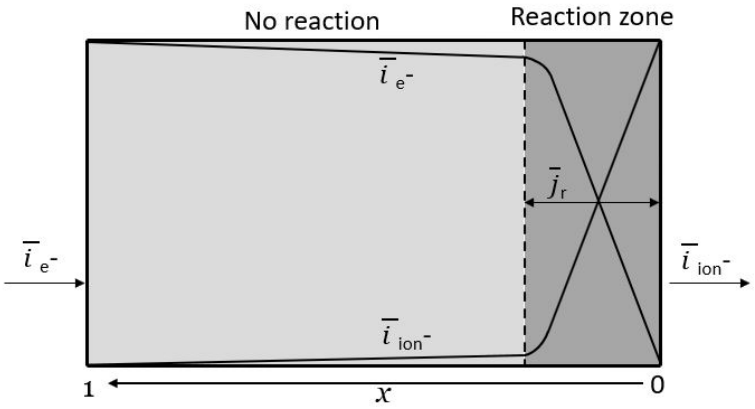

Figure 3.1: Schematic of equation 3.14, $\bar{j}_r$ indicates the reaction zone, were the conversion takes place. At $x = 0$ is the membrane and at $x = L$ is the current collector, $\bar{i}_{e^-}$ and $\bar{i}_{ion^-}$ represent the current in the electrode and electrolyte respectively.

Concentration Polarization

The Tafel regime represents a simplification of the Butler-Volmer equation at high overpotentials $\bar{\eta} > 1$ or currents exceeding the exchange current density $\bar{j}_* > 1$. However, this is not always the case; it is also interesting to know what happens at lower potentials, which are more favorable when taking into account the efficiency.

$$\bar{i}' = \frac{\bar{c}}{\bar{j}_r} = \frac{(1-\bar{c})e^{\bar{\eta}} - \bar{c}e^{-\bar{\eta}}}{\bar{j}_*} \tag{3.16}$$

When multiplying by $\bar{j}_*$, $\frac{\bar{c}\bar{j}_*}{\bar{j}_r}$ reduces to almost zero since both $\bar{j}_*$ and $\bar{c}$ are very small. Using this results into the following equation:

$$(1-\bar{c})e^{\bar{\eta}} = \bar{c}e^{-\bar{\eta}} \tag{3.17}$$

Which can be rewritten into a function for the overpotential:

$$\bar{\eta} = \ln\left(\left(\frac{\bar{c}}{1-\bar{c}}\right)^{\frac{1}{2}}\right) = \ln\left(\left(\frac{\bar{j}_r}{1-\bar{j}_r}\right)^{\frac{1}{2}}\right) \tag{3.18}$$

when j approaches 0, the overpotential is not determined by ohmic losses, as is the case with the Tafel kinetics, but rather by a change in equilibrium potential. Meaning the distance to the membrane is less important compared to the local concentration. Therefore, at low currents the concentration of the oxidized mediator is homogeneously spread through the electrode. Consequently, $\bar{j}_r$ translates the current into an average concentration, thus $\bar{j}_r = \bar{c}$. equation 3.18 can also be rewritten in dimensional terms:

$$\Delta V = b \ln\left(\sqrt{\frac{j}{kc_0FL\epsilon - j}}\right) \tag{3.19}$$

Combined Solution

The solutions acquired from both the Tafel and the concentration polarization regime can be combined by using their effectiveness factors:

$$\Delta\bar{V} = \ln\left(\sqrt{\frac{\bar{j}_r}{1-\bar{j}_r}} + \frac{\bar{j}_*}{\mathcal{E}_{\text{Tafel}}}\right) + \bar{j}_{\kappa+\sigma} = \ln\left(\sqrt{\frac{\bar{j}_r}{1-\bar{j}_r}} + \bar{j}_* \frac{e^{\frac{\bar{j}_r\bar{j}_\kappa}{2}} - 1}{\bar{j}_r}\right) + \bar{j}_{\kappa+\sigma} \tag{3.20}$$

Equation 3.20 offers a solution for the full range of current densities, at low currents the left term in the natural logarithm is dominant and at higher currents the right is more dominant. When converted back to dimensional form:

$$\Delta V = b \ln\left(\sqrt{\frac{kc_0FL\epsilon}{j}} + \frac{e^{\frac{j^2}{2kc_0\epsilon\kappa}} - 1}{\frac{k\epsilon}{k_0a_v}}\right) \tag{3.21}$$

With Mass Transfer

The problem with the derivation above is that $\bar{j}_r$, defined in equation 3.2, assumes a maximum current where the entire pore volume is filled with the oxidized mediator, enabling maximum chemical conversion. However, this is only the case when $k_m a_v \gg k\epsilon$

Instead of marking the chemical reaction as limiting, mass transport could become limiting. Generally, mass transfer is modeled in series with either an electrochemical or a chemical reaction. This research models both, meaning that the mass transfer is in series and parallel to the chemical reaction. Here the Hatta analysis comes in which is discussed in section 2.3.5. The Hatta analysis introduces an enhancement factor, quantifying the extra mass transfer due to the chemical reaction between the bulk and the electrode surface. To adjust for the mass transfer $\bar{j}_r$ in equation 3.20 needs to be replaced by $\bar{j}_m$ which is the current normalized by the maximum current density achievable due to mass transfer given by:

$$\bar{j}_m = \frac{j}{j_m} \quad \text{,where} \quad j_m = N_m F L a_v \tag{3.22}$$

Where, N_m is defined in equation 2.36, this leads to a new equation for the overpotential of:

$$\Delta\overline{V} = \ln\left(\sqrt{\frac{\bar{j}_m}{1-\bar{j}_m}} + \bar{j}_* \frac{e^{\frac{\bar{j}_m \bar{j}_\kappa}{2}} - 1}{\bar{j}_m}\right) + \bar{j}_{\kappa+\sigma} \tag{3.23}$$

3.2. 2D model

For the 2D model COMSOL was chosen, a multi-physics software package, capable of simulating and combining different physical phenomena, and able to do so in multiple dimensions. A key motivation for using COMSOL is its ability to combine flow, chemical and electrochemical reactions in porous media. Also, its large number of available tutorials on the electrochemical module, together with its broad userbase in the industry.

Firstly, the input parameters will be presented. Secondly, the governing equations and boundary conditions are discussed. Thirdly, this section elaborates upon the additional assumptions that needed to be made in order for the model to function. Finally, the mesh is considered.

3.2.1. Parameters

Throughout the theory section constants are presented in tables, which all serve as input to the COMSOL model. The kinetics and the diffusion coefficients of TEMPO and ACT are presented in table 2.1 and 2.2. The rate constants of the chemical reactions can be found in table 2.3. The equilibrium reaction of the buffer can be found in table 2.4. Nevertheless, there is still more input needed in terms of geometry, conditions, material properties, inlet conditions and the diffusion coefficients of the molecules used. These are shown in tables 3.2 and 3.3.

Input type	Parameter	symbol	value	unit
Geometric	Height of cell	h	0.1	[m]
	Width of cell	w	0.1	[m]
	Thickness of anode	L	4	[mm]
Material properties	Porosity	ϵ	0.95	[-]
	Electrode conductivity	σ	150000	[S/m]
	Electrolyte conductivity	κ	5	[S/m]
Process	Temperature	T	293.15	[K]
	Flow velocity	u	0.0035	[m^2/s]
	Current density	j	var	[A/m^2]
Inlet conditions	Tempo concentration	c_{Tempo}	40	[mol/m^3]
	PDO concentration	c_{PDO}	200	[mol/m^3]
	H3BO3 concentration	c_{H3BO3}	300.15	[mol/m^3]
	H4BO4 concentration	c_{H4BO4}	199.15	[mol/m^3]

Table 3.2: Parameters used as input in COMSOL.

Chemical	Diffusion coefficient (D) 10^9 [m^2/s]	source
ACT	0.33	Pérez-Gallent et al. [47]
PDO	1.14	Wang[58]
LA	1.03, 1.00	CNC handbook[59], Koerlsch2013[36]
PA	1.12	Koerlsch
H_3BO_3	1.3	CNC handbook
$H_4BO_4^-$	1.3	CNC handbook
OH^-	5.27	CNC handbook

Table 3.3: Diffusion coefficients of the species used in COMSOL.

3.2.2. Boundary Conditions, Simulation Settings and Assumptions

The first step in building a COMSOL simulation is to chose the right modules. Each module represents a certain discipline in physics. For this model the following modules were chosen, accompanied with their governing equation:

Current Distribution

A secondary current distribution is chosen because of the use of the buffer which also serves as a supporting electrolyte, with a constant conductivity [2]:

$$i_{\text{ion}^-} = -\kappa \nabla \phi_{\text{ion}^-}, \tag{3.24}$$

secondly since the kinetics of the of the oxidation of the mediator are not reversible, the kinetics are potential driven like in equation 3.25.

$$j_{\text{loc}} = j_{**}\left(\frac{c_o}{c_{o,\text{eq}}} e^{-\left[\frac{\alpha F \eta}{RT}\right]} - \frac{c_r}{c_{r,\text{eq}}} e^{-\left[\frac{(1-\alpha) F \eta}{RT}\right]} \right), \tag{3.25}$$

where j_{loc} is the local current density.

Mass Transport

The mass transport is done with the module of *transport of diluted species in porous media*. Which is a macroscopic representation of the mass transport. It is done using the following equation[3]:

$$\frac{\partial}{\partial t}(\epsilon c_i) + \mathbf{u} \cdot \nabla c_i = \nabla \cdot [(D_{\text{D},i} + D_{\text{e},i}) \nabla c_i] + R_i + S_i \tag{3.26}$$

where, **u** is the 2 dimensional superficial flow speed and D_{D} is the dispersion, which is not used in this research. R_i and S_i are the reaction and source term respectively.

Hydrodynamics

For the hydrodynamic part, the Brinkman equation is used, which describes "(...) fast-moving fluids in porous media with the kinetic potential from fluid velocity, pressure, and gravity to drive the flow. These equations extend Darcy's law to describe the dissipation of the kinetic energy by viscous shear as with the Navier-Stokes equations."[3]:

$$\rho \frac{\partial \mathbf{u}}{\partial t} - \mu(\nabla \mathbf{u} + (\nabla \mathbf{u})^T) - \left(\frac{\mu}{K} \mathbf{u} + \nabla p - \mathbf{F} \right) = 0 \tag{3.27}$$

$$\nabla \cdot \mathbf{u} = 0 \tag{3.28}$$

Here, μ is the dynamic viscosity and K is the permeability. Permeability is dependent mainly on the porosity and pore size of the porous medium.

Boundary Conditions

Besides the right modules, accompanied by their governing equations, the following boundary conditions (BC) were established:

- A slip boundary condition on the current collector and membrane walls, since the Brinkmann equation already resolves the friction;
- Danckwerts inlet BC [14], which ensures the concentrations do not drop below zero at the inlet;
- OH^- flux from the membrane proportional to the current, this way, the conservation of charge is maintained, simulating the hydroxide that would otherwise pass through the membrane;
- The potential at the membrane is set at zero; this implies that the potential at the current collector is the applied potential to the half cell.

All simulation- and boundary conditions are displayed in Figure 3.2.

Additional Assumptions
Besides the assumptions made in the simulation settings and boundary conditions discussed above, the model contains several additional assumptions:

- The reactor is in steady state;
- The model is isothermal, meaning the temperature does not change;
- There are no microscopic mass transfer effects, meaning there is no mass transport limitation in the pores;
- Only the anode is considered, not the cathode;
- The inlet is considered to be fully developed.
- Faradaic losses are not considered.

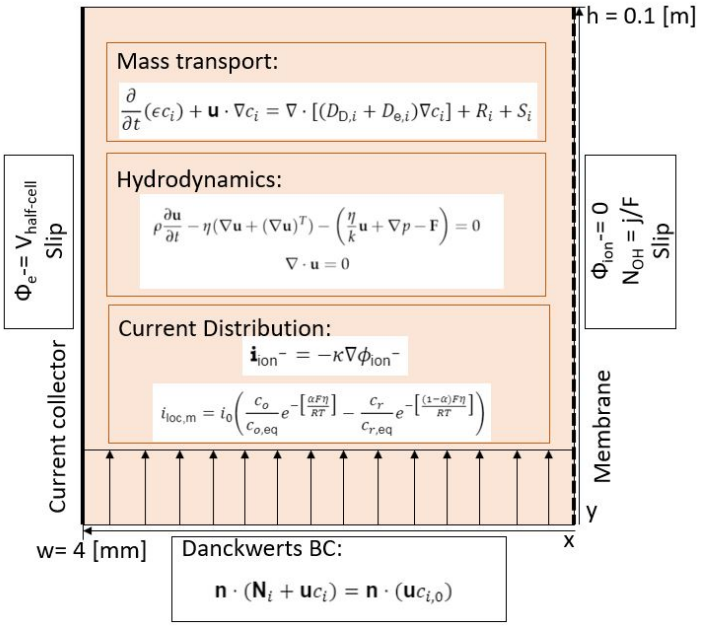

Figure 3.2: Overview of the used governing equations and boundary conditions.

3.2.3. Meshing

COMSOL solves physical problems using a finite element method. These elements combined form a mesh, such as shown in Figure 3.3. The accuracy of the simulation is heavily dependent on how fine the mesh is made. A finer mesh leads to a more accurate solution, but it will also take longer to compute. Therefore, one should strive for a mesh resolution that provides an accurate solution, but that is not unnecessarily accurate, making it computationally expensive. One way to do so is to create a mesh with varying resolutions based on the required accuracy at specific places in the domain. Higher accuracy can be needed, for instance, at the inlet or places with high gradients in concentration or velocity. Generally speaking, the mesh should be fine where a property (e.g., concentration, velocity) is subject to change. In the porous electrode, this is at the membrane and the inlet. Therefore, the mesh in this report is more refined in these areas, as shown in Figure 3.3.

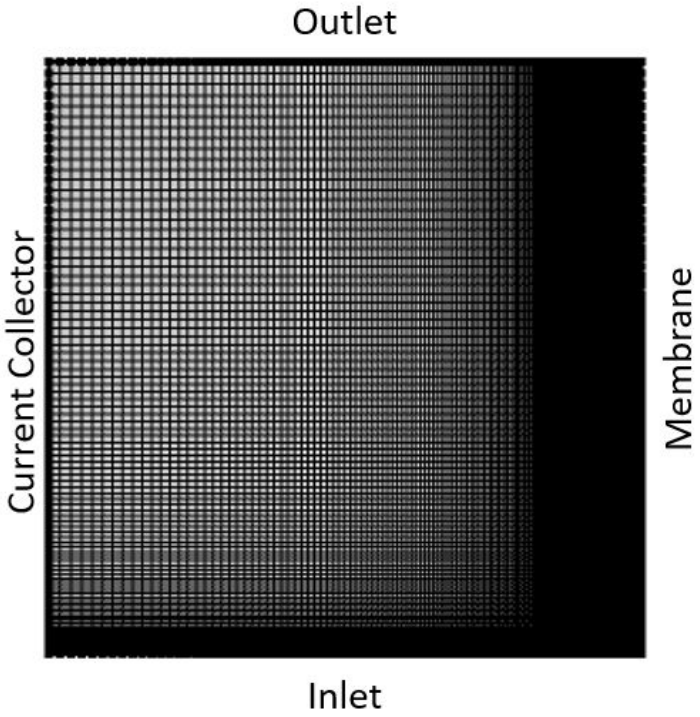

Figure 3.3: A 200x100 where the elements are distributed more towards the membrane and the inlet.

4

Results & Discussion

4.1. 2D model Validation

This section analyses the results of the 2D model. First, the mesh is analyzed to examined whether the solution changes with different mesh resolutions. Second, the results of the 2D model are reviewed.

4.1.1. Mesh Resolution

First, the 2D model mesh is checked on whether the mesh fineness affects the solution the 2D model provides. This is done by testing different mesh resolutions; the resolutions used are provided in table 4.1.

The outcomes of the different mesh resolutions are plotted in Figure 4.1.

	Coarse	Fine	Finer	Finest
number of cells among anode height	50	100	150	200
number of cells in width of anode	100	200	300	400
total number of cells	5000	20000	45000	80000

Table 4.1: Mesh resolutions used to check model for mesh dependence.

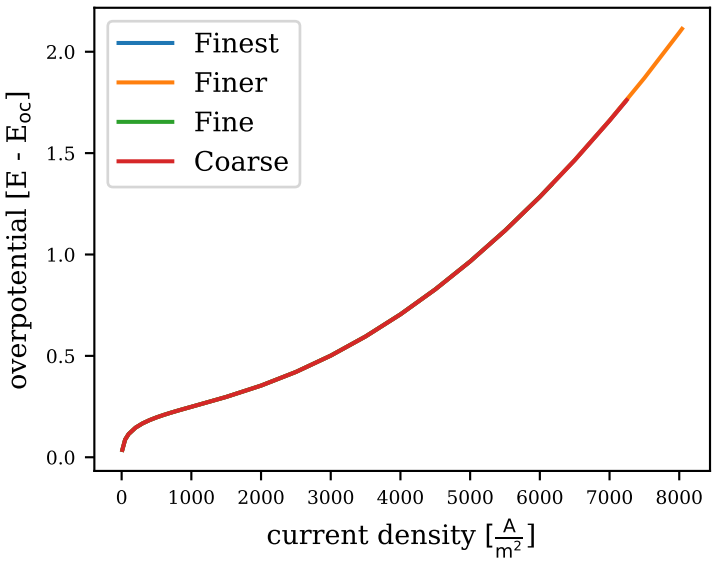

Figure 4.1: Overpotential vs. current solution for each mesh resolution proposed in table 4.1. Graph shows perfect overlap. The finer and finest meshes are more stable and achieve higher current densities compared to the fine and coarse mesh.

4.1.2. 2D Model Results

The 2D contains eight species in the electrolyte with each of their characteristics amounting to over 30 parameters. Here the results of this model are analyzed and checked on reasonability.
First, since the electrode is a lot more conductive than the electrolyte, it is expected that the reaction takes place close to the membrane. In other words, the PDO converts close to the membrane, whereas, at the current collector, no conversion occurs. To achieve conversion, $TEMPO^+$ is required since the rate is dependent on it. Figure 4.2 shows the resemblance of the model with the criteria mentioned above.

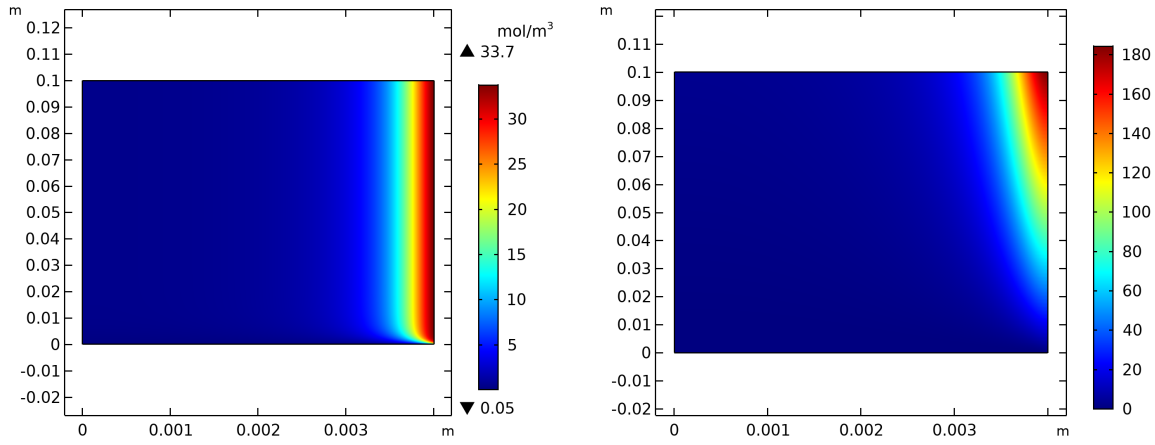

(a) $TEMPO^+$ concentration at a current density of 1500 $\frac{A}{m^2}$

(b) LA concentration at a current density of 1500 $\frac{A}{m^2}$

Figure 4.2: Two surface plots of both $TEMPO^+$ and LA, at 1500 $\frac{A}{m^2}$ and a flow speed of 0.0035 $[\frac{m}{s}]$ in a 4 mm thick electrode. In each figure the membrane is depicted on the right and the current collector on the left.

As mentioned in the TEMPO section 2.1.4, the pH should be kept in a particular range for TEMPO to remain stable. Also, as argued in section 2.3.4, the ability of the buffer to maintain the pH is dependent on the current and the flow velocity. Figure 4.3 shows the local pH inside the electrode, on the left, in Figure 4.3a the local pH at a current of 1500 $[\frac{A}{m^2}]$ and a flow speed of 0.0035 $[\frac{A}{m^2}]$ are presented. On the right, in Figure 4.3b, shows the same current with a flow speed of 0.1 $[\frac{m}{s}]$, proving that stable pH at the membrane is not obvious.

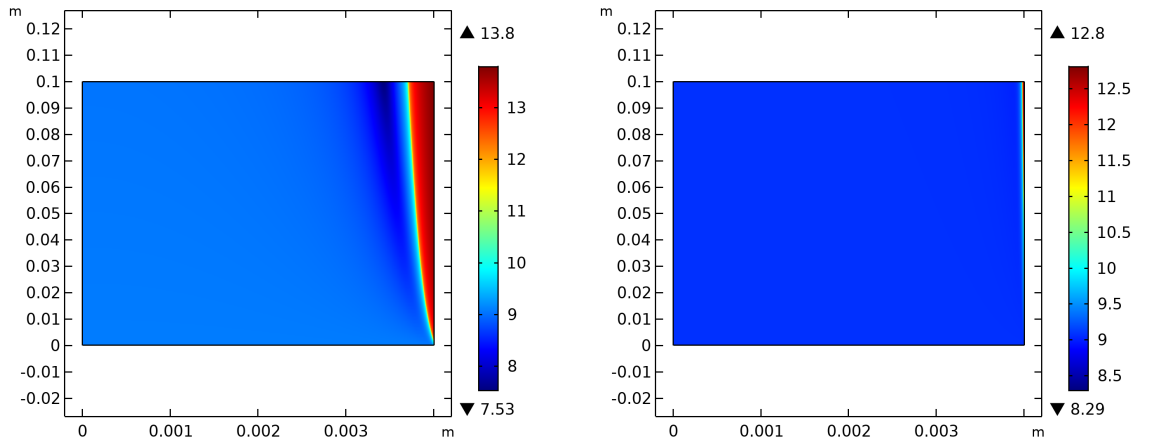

(a) surface plot of the pH at a current density of 1500 $[\frac{A}{m^2}]$ at a flow velocity of 0.0035 $[\frac{m}{s}]$.

(b) surface plot of the pH at a current density of 1500 $[\frac{A}{m^2}]$ at a flow velocity of 0.1 $[\frac{m}{s}]$.

Figure 4.3: Two surface plots of the pH at flow velocities of 0.0035 and 0.1 $[\frac{m}{s}]$ and both at a current density of $[\frac{A}{m^2}]$. In each figure the membrane is presented on the right and the current collector on the left. The buffer used is a 0.5 M Boric acid buffer. In Figure (a), it is visible that the buffer is depleted due to the high pH in a relatively large area. In Figure (b), there is also depletion; however, the depletion area is less compared with Figure (a).

Last to consider are the flow velocity and the pressure drop across the electrode. Since it is a porous material, uniform flow is expected, meaning that the flow speed is the same everywhere, and the pressure decreases linearly with the length of the reactor. Figure 4.4a shows the velocity, which indeed is uniform. Figure 4.4b shows the pressure drops, which decreases with the length of the reactor.

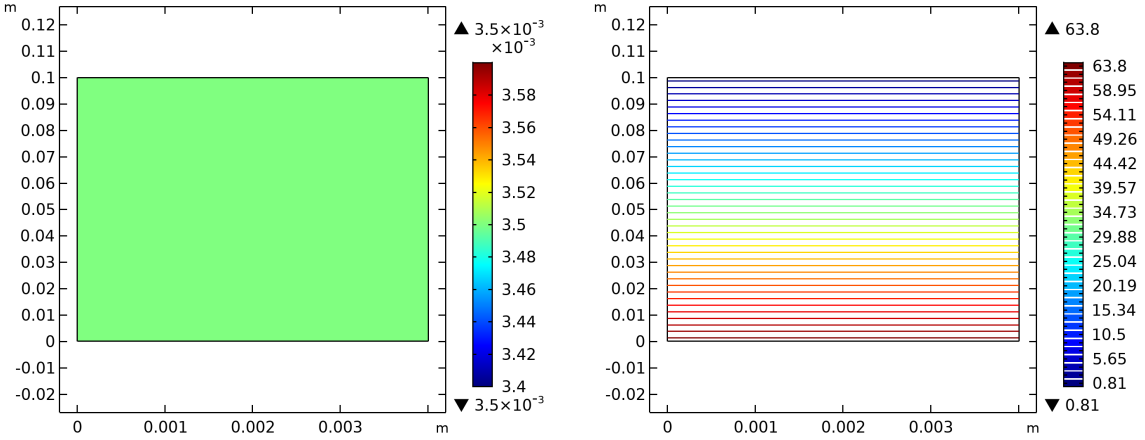

(a) Surface plot of the flow velocity in the porous electrode, clearly indicating a constant velocity throughout the domain

(b) Contour plot of the pressure drop, showing a linear decline along the length of the electrode.

Figure 4.4: A surface plot of the flow velocity in the electrode and a contour plot of the pressure drop. In both figures the membrane is depicted on the right and the current collector on the left.

4.2. Analytical Model Validation

The analytical model is validated with the 2D model; the formula validated is equation 3.20. First, equation 3.18 is investigated, second the validity in the Tafel regime of equation 3.14 is checked and finally, a sensitivity analysis is done by varying the parameters in equation 3.20

4.2.1. Concentration Polarization

This section investigates, the validity of equation 3.18 by checking if the normalized concentration is equal to the current normalized by the maximum reaction rate: $\bar{c} = \bar{j}_r$. First, the concentration profile of TEMPO$^+$ was extracted from COMSOL and normalized with Tempo's initial concentration. Second, $\bar{j}_r$ was calculated, by equation 3.2, for each current. Both are plotted in Figure 4.5. In the left Figure 4.5a current densities 1 and 10 $[\frac{\text{A}}{\text{m}^2}]$ are compared, here the assumption, $\bar{c} = \bar{j}_r$, shows good agreement. In the right Figure 4.5b, slightly elevated current densities are plotted: 50, 100, and 200 $[\frac{\text{A}}{\text{m}^2}]$, of which 50 $[\frac{\text{A}}{\text{m}^2}]$ show reasonable agreement whereas, for 100 and 200 $[\frac{\text{A}}{\text{m}^2}]$, there is little agreement. The disagreement is probably caused by the neglected ohmic loss in the electrolyte by equation 3.18. Here, the reaction's position is determined more by the ohmic losses rather than by the activation loss. Therefore, the assumption is only valid when $\bar{j}_\kappa < 1$, which is true for small current densities such as: 1, 10 and, 50 $[\frac{\text{A}}{\text{m}^2}]$.

4.2.2. Tafel

This section examines the validity of equation 3.14 against the 2D model. As stated in section 3.1.3 the dominant term in this equation is: $\frac{\bar{j}_r \bar{j}_\kappa}{2}$, where the $\bar{j}_r$ describes the electrode utilization from the membrane into the electrode, shown in Figure 3.1. In order to validate, concentration profiles of TEMPO$^+$ at different current densities are extracted from COMSOL. Figure 4.6a shows the TEMPO$^+$ concentration of the whole electrode. However, this figure cannot be used to compare different current densities. Therefore, the concentration profiles are extracted along the green dashed line of Figure 4.6a and plotted as solid lines in Figure 4.6b. Also, $\bar{j}_r$ is plotted as a dashed line in the color corresponding to the current densities; 2000, 4000, and 6000 $[\frac{\text{A}}{\text{m}^2}]$. Figure 4.6b, proves that j_r indeed indicates the end of

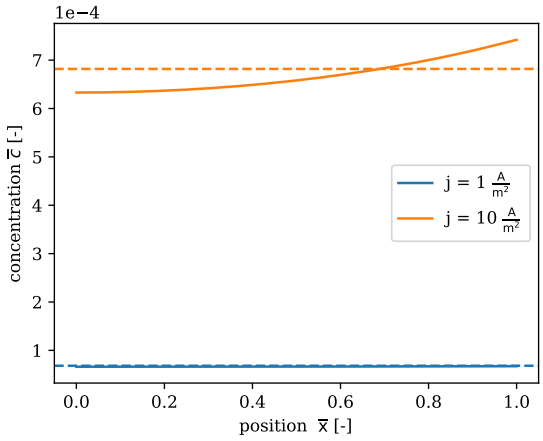

(a) normalized concentration profile of TEMPO+ at 1 and 10 $[\frac{A}{m^2}]$

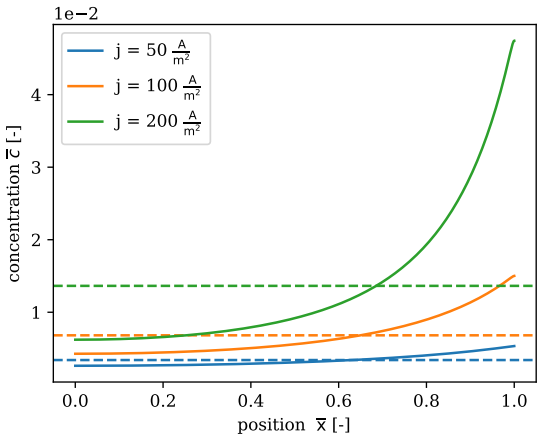

(b) normalized concentration profile of TEMPO+ at 50, 100 and 200 $[\frac{A}{m^2}]$

Figure 4.5: The normalized concentration profile of TEMPO+ at 1, 10, 50, 100 and 200 $[\frac{A}{m^2}]$, the solid line is generated by COMSOL and the dashed line is $\bar{j}_r$. $\bar{x}$=1 is at the membrane and $\bar{x} = 0$ is at the current collector.

the reaction zone. Although the position where j_r intersects the line is not at $\bar{c} = 1$, the intersection point does not change with the current density.

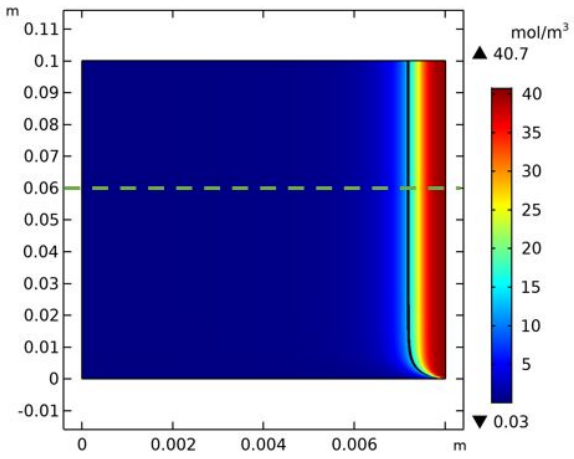

(a) Concentration profile of TEMPO+ at 3000 $[\frac{A}{m^2}]$ generated by COMSOL, where the dashed green line indicates the line along which the profiles of Figure 4.6b are extracted.

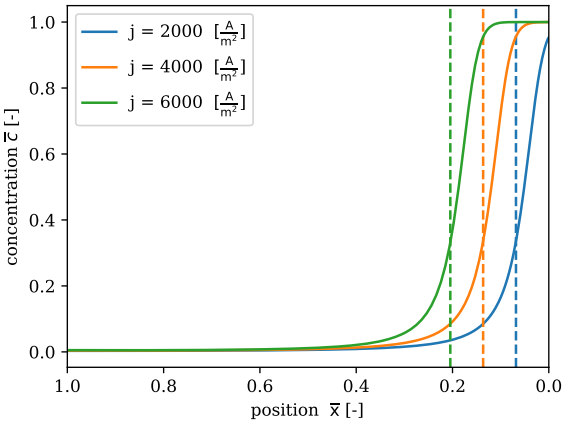

(b) The solid line is the concentration profile extracted from the horizontal dashed green line in Figure (a). Here the vertical dashed lines represents j_r at the current density associated with its color.

Figure 4.6: Figure (a) is extracted from the COMSOL model, the horizontal dashed green line indicates the line along which the profiles of Figure (b) are extracted. Figure (b) compares $\bar{j}_r$, indicated by the vertical dashed lines, with the profiles, showing good agreement

4.2.3. Sensitivity Analysis

To verify whether the analytical model varies in similar fashion as the 2D model. The parameters of equation 3.21, consisting of the rate constant k, electrolyte conductivity κ, and initial mediator concentration c_0, are varied. First, the chemical rate constant is varied in Figure 4.7a. The default parameters used can be found in table 4.2. The potenital reported in the figures it the potential minus the standard potential which is when $\bar{c} = 0.5$. When the current density is close to zero $\bar{c} \approx 0$, causing a shift in equilibrium potential and thus resulting in a negative potential for low current densities, as shown in Figure 4.6.

Figure 4.7a shows good agreement between the analytical and 2D model. At higher current densities, the analytical solution slightly overestimates at a high rate constant and slightly underestimates at a low rate constant. In the range between 100 and 1000 $[\frac{A}{m^2}]$ the agreement with the analytical solution

Default parameters			
k [m/s]	L [mm]	c_0 [mol m^{-3}]	κ [S/m]
1	4	40	5

Table 4.2: Default parameters of both the analytical and the 2D model.

and the 2D model for $k = 0.5$ is off. The current density range corresponds to the transition between the polarization concentration and Tafel regime, this might cause the disagreement.
In Figure 4.7b, the initial mediator concentration is varied between 15 and 100 [mol m^{-3}]. Here the analytical model and the 2D model are in near-perfect alignment.
Figure 4.7c the electrolyte conductivity κ is varied between 1 and 50 [S/m]. The analytical solution underestimates the COMSOL model slightly for all the conductivities but follows the same trend. Concluding on from the graphs in Figure 4.7, the analytical model varies in the same way as the 2D model. Besides some slight under- and overestimation, there is a good agreement.

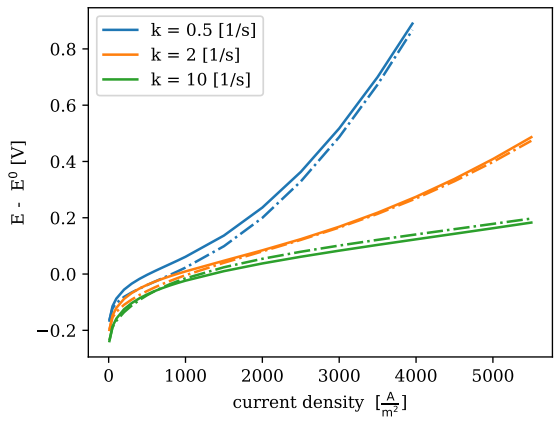

(a) The rate constant k was varied, while keeping the other parameters of table 4.2 constant.

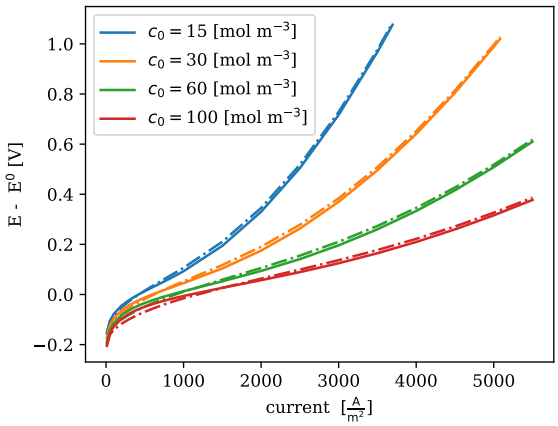

(b) The initial Tempo concentration c_0 was varied, while keeping the other parameters of table 4.2 constant.

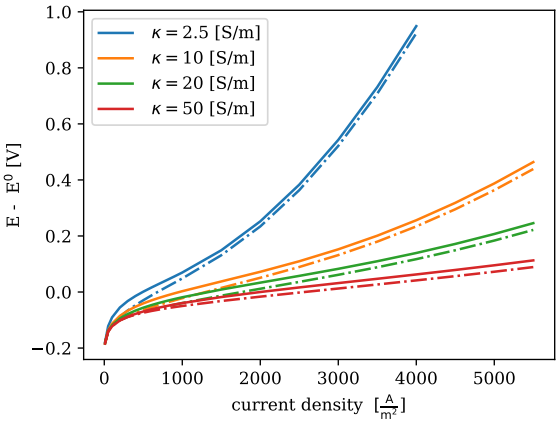

(c) The electolyte conductivity κ was varied, while keeping the other parameters of table 4.2 constant.

Figure 4.7: Overpotential vs. current result comparison between the COMSOL model and the analytical model, where in Figure a, b and c the rate constant k, initial Tempo concentration c_0 and electrolyte conductivity κ was varied respectively, while the rest of the parameters were kept at their default values as presented table 4.2

4.3. Optimization

This section researches what parameters to focus on when optimizing a reactor based on the models. The 2D model may be more accurate; however it is less insightful as well. It is only evident what the effect of a parameter variation is after it has run. In the analytical model, the effect is immediately visible

prior to any calculation. In addition to its correspondence with the 2D model, shown in section 4.2.3, it moreover provides an insightful tool to optimize a reactor. With the analytical solution. First, a reactor is considered without any mass transport limitations, then with mass transfer limitations, and finally, metal foams and the mediator's effect is analyzed.

4.3.1. Optimization without Mass Transfer

In this section the pore volume is assumed to be perfectly mixed. The flow velocity does not influence mass transfer and thus does not change the potential-current relation of equation 3.20. The sole purpose of the flow is to maintain sufficient substrate levels to sustain a reaction. When assuming a particularly soluble substrate, only a little flow is required, causing a low pressure drop which in turn yields negligible pumping losses. When pumping losses are not considered, the only way to improve the efficiency of a reactor is to lower the overpotential required to reach a certain current density. Another assumption made here is that the reactor, for it to be economically viable, runs at current densities above 1000 [A/m^2]. Following equation 3.14, $e^{\frac{\bar{j}_r \bar{j}_k}{2}} \gg 1$, meaning that ohmic losses are the main contributor to the overpotential. Together with the assumption that the pore volume is perfectly mixed, this assumption leads to the following equation for the overpotential in the reactor:

$$\Delta V \approx \frac{j^2}{k c_0 \varepsilon F \kappa}, \tag{4.1}$$

Efficiency ε, is used to quantify the performance of the reactor. The efficiency is calculated by dividing the useful energy by the total energy put into the system:

$$\varepsilon = \frac{P_{\text{useful}}}{P_{\text{total}}} = \frac{E_{\text{a}} j}{E_{\text{a}} j + \Delta V j} = \frac{E_{\text{a}}}{E_{\text{a}} + \frac{j^2}{k c_0 \epsilon F \kappa}}, \tag{4.2}$$

where, the useful energy, P_{useful}, is based on the activation potential of the mediator times the current density. The total energy consists of the useful energy and the overpotential, times the current density. Together with the relation for the overpotential, the efficiency is defined in equation 4.2. The equation shows that in order to increase the efficiency, the mediator concentration, porosity, rate constant, and electrolyte conductivity need to be increased. Interestingly, the thickness does not influence the performance of the cell. However, in order to not waste material the minimal electrode thickness can be found by: $L = \frac{j}{k c_0 F \epsilon}$. The only geometrical property directly influencing the cell's efficiency is ϵ. With the assumptions made, the properties of the mediator are determining for the reactor's performance.

4.3.2. Optimization with Mass Transfer

Without mass transfer, optimizing gets more tedious. Now, there is an extra step between and parallel to the oxidation on the electrode surface and the bulk reaction. Equation 3.23 describes this relationship. Mass transfer can be a limiting factor in reaching high currents at reasonable overpotentials. It depends on the flow speed, the geometry of the reactor, and the mediator's diffusivity. Increasing the speed of the flow yields more mass transfer and thus a lower overpotential for the same amount of current. However, the increased flow speed also induces a higher pressure drop and, therefore, higher pumping losses. To optimize the reactor, the pumping losses must be included, which can be calculated by equation 4.3:

$$P_{\text{pump}} = \Delta p u L w = \frac{h f \mu u}{d_{\text{eq}^2}} u L w = \frac{f \mu L u^2 w h}{d_{\text{eq}^2}}, \tag{4.3}$$

where Δp is the pressure drop calculated by the equations in section 3.1.2, u the flow velocity, L the thickness of the electrode, h the length of the electrode and w the width of the electrode. When using equation 4.3 for the efficiency, the pump loss needs to be divided by the projected area of the cell. This leads to the following equation for the efficiency:

$$\varepsilon = \frac{P_{\text{useful}}}{P_{\text{total}}} = \frac{E_{\text{a}} j}{E_{\text{a}} j + \frac{j^3}{k_m \Theta F a_v \kappa (1 - \frac{a_v \Theta k_m}{a_v \Theta k_m + k \epsilon (1 - \frac{1}{\text{AL}})})} + \frac{\mu f L u^2}{d_{\text{eq}}^2}}. \tag{4.4}$$

Equation 4.4 explains how the efficiency can be calculated. Note that instead of ϵ now a_v is the geometrical parameter that needs to be maximized compared to the model without mass transfer. Moreover, the formula for the minimal electrode thickness changes into: $L = \frac{j}{k_m \Delta c \Theta F a_v}$. In order to find the optimum flow velocity for a particular current, the derivative must be taken with respect to the flow speed, u, since k_m and f are dependent on the flow velocity as well. The formula that would be derived would be so complex that it would not yield any insights. Therefore, the optimization is done numerically, by calculating different currents for every flow speed, comparing the efficiencies, and choosing the optimal current velocity combination. This process is graphically shown in Figure 4.8. This process is also used in the results of the following section.

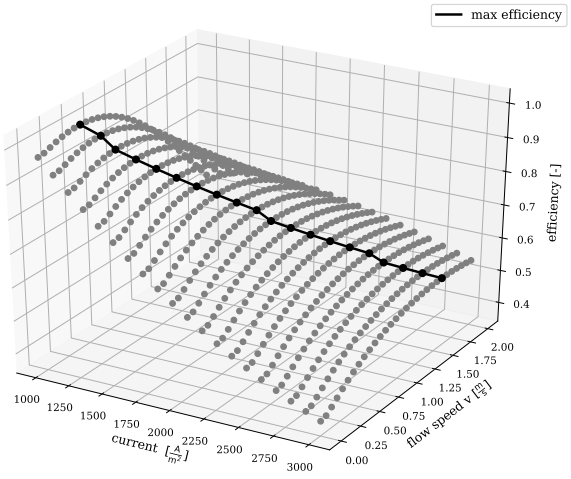

Figure 4.8: 3D plot where every grey dot represents a the efficiency of a combination of a flow speed and current. The black line represents the optimal combination of current and flow speed. This graph is based on: a foam with a porosity $\varepsilon = 0.95$, volumetric surface area , a_v = 5600[1/m], thickness, L = 4 [mm] and a mediator with a rate constant $k = 5$ [S/m] and Diffusion coefficient $D = 3.3\,10^{-10}$ [m^2/s]

4.3.3. Foams

For the study, three metal foams are used. The same geometry is used as proposed in Table 3.2. The metal foams are nickel foams from Recemat BV [1]. Their properties are provided in Table 4.3:

Designation	Ni-2733	Ni-4753	Ni-5763
Pores per inch	27...33	47...53	57...63
average pore diameter [mm]	0.6	0.4	0.35
porosity	95.2%	95.2%	96%
Volumetric surface area [1/m]	2800	5400	6900

Table 4.3: Nickel foam properties extracted from the website of Recemat BV [1].

When comparing the metal foams there are three variables: pores per inch, average pore diameter, and the volumetric surface area. The volumetric surface area is used as an input parameter. The other two are related to it. Thus only using the volumetric surface area to differentiate between the foams seems like a legitimate assumption.
Now, using the same method as described in section 4.3.2 Figure 4.9 is created. Note that for every current, the ideal flow speed is used. Therefore, it is a 2D plot instead of 3D, which yields better readability.

Figure 4.9 shows that a higher volumertic surface area yield a higher efficiency. It is key to note however, since an increase in volumetric surface area does not effect the porosity there is no optimal volumetric surface area. In reality at one point porosity should decrease when surface area increases,

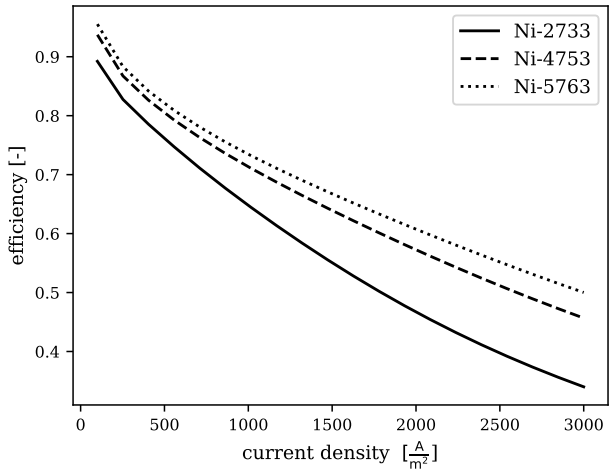

Figure 4.9: Foams of table 4.3 with a mediator with a rate constant, k of 5 [1/s], Diffusion coefficient D of $3.3\,10^{-10}$[m^2/s] and the thickness of the foam, L = 4 [mm]

otherwise the strut thickness would become to small following the formula of Lacroix et. al. The relationship between surface area and porosity is material dependent and to maintain general applicability, it was excluded.

4.3.4. Mediator

Equation 4.4 shows that the reactor's efficiency depends substantially on the mediator properties. This section examines the mass transport of the mediator in the porous electrode.
When considering the Hatta analysis for the mass transfer, there are two regimes. Firstly, the reacting-diffusion regime, in which the oxidized mediator is reduced again before reaching the bulk. Secondly, the reacting-diffusion-advection, in which the reaction occurs both in the mass transfer boundary layer and in the bulk. Of these two, the reacting-diffusion-advection is the most complex to generalize. For this analysis the following equations were used: 3.23 combined with equations, 2.32 and 2.33. When using these equations, one should always ensure that the conditions for simplification still hold: AL $\gg$ 1 and (1-AL)Ha^2 $\gg$ 1. If they do not hold, one should use the extensive equation 2.30 also in section 2.3.5. The reacting-diffusion regime is where the catalytic, very active mediators will be in. In comparison, the reacting-diffusion-advection regime is more important for mediators with a more moderate catalytic activity.

Reacting-Diffusion

When Ha$\geq$ 2, which only occurs at particularly low flow velocities or at a high rate constant, tanh(Ha) becomes 1. Therefore, equation 4.5 simplifies to the Hatta number:

$$\Theta = \frac{\mathrm{Ha}}{\tanh(\mathrm{Ha})} \propto \mathrm{Ha} = \frac{\sqrt{kD}}{k_m}. \tag{4.5}$$

When this enhancement factor is used in equation 2.33 and then put into equation 3.14, the following approach to the overpotential is obtained:

$$\Delta V \approx \frac{j^2}{k_m \Delta c \frac{\sqrt{kD}}{k_m} F a_v \kappa} = \frac{j^2}{\sqrt{kD} c_0 F a_v \kappa} \tag{4.6}$$

Note that the mass transfer coefficient drops out. The Hatta number can also be seen as a ratio between the mass transfer boundary layer and the diffusion-reaction boundary layer. In this case, when the diffusion-reaction layer is smaller than the mass transfer boundary layer, hence Ha $\geq$ 2, there will be no mass transfer towards the bulk anymore since the mediator is already reduced inside the reacting boundary layer. This means that when Ha $\geq$ 2, this can be either due to a low velocity or to a very reactive mediator.

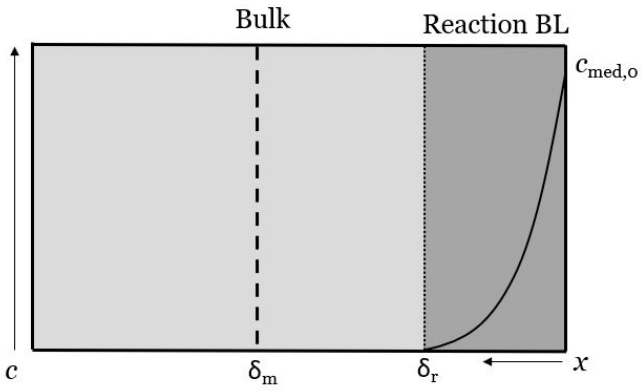

Figure 4.10: Schematic of porous electrode, with two boundary layers, the reaction boundary layer indicated by δ_r and the convective boundary layer indicated by δ_m. $x = 0$ indicates the electrode surface. Here the Hatta number Ha ≫2, resulting in reaction boundary layer smaller than the convective boundary layer and thus the oxidized mediator does not reach the bulk.

Diffusion-Reaction-Advection

It gets more tedious when the mass transfer boundary layer is smaller than the reaction-diffusion boundary layer. In that case where $0 < \text{Ha} < 2$ and thus the enhancement is $1 < \Theta < 2$, the overpotential scales with equation 4.7:

$$\Delta V \approx \frac{j^2}{k_m c_0 \Theta F a_v \kappa (1 - \frac{a_v \Theta k_m}{a_v \Theta k_m + k\epsilon(1-\frac{1}{AL})})}. \tag{4.7}$$

The formula shows that increasing the electrolyte conductivity, volumetric surface area, and the mediator concentration results in lower overpotential losses. About the mass transfer coefficient such a statement cannot be made. The effect on the overpotential of increasing the mass transfer depends on the ratio between the mass transfer and the rate constant. If the mass transfer is increased, but it is already high compared with the rate constant, it will also lead to lower concentration gradients between the wall and the bulk leading to less mass transfer. This can be quantified by equation 4.8, already introduced in section 2.3.5:

$$(1 - \text{AL})\text{Ha}^2, \tag{4.8}$$

similar to van Elk et al. [56] equation 4.8 can provide insight into ”the ratio of the maximum conversion in the liquid bulk to the maximum transport through the film”. Meaning that when $(1 - \text{AL})\text{Ha}^2 < 1$ the bulk is saturated with oxidized mediator and the chemical reactor can be considered rate limiting. When $(1 - \text{AL})\text{Ha}^2 \gg 1$ the mass transfer is rate limiting, and increasing the flow velocity will result in a higher achievable current density.

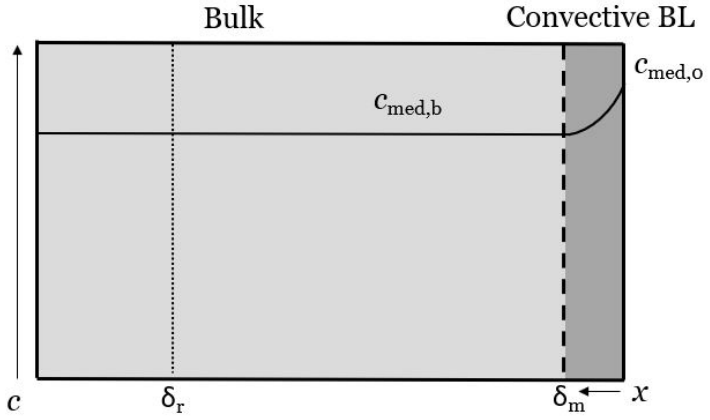

Figure 4.11: Schematic of porous electrode, with two boundary layers, the reaction boundary layer indicated by δ_r and the convective boundary layer indicated by δ_m. $x = 0$ indicates the electrode surface. Here the Hatta number Ha <1, resulting in an advective boundary layer significantly smaller than the reaction boundary layer.

Conclusion on Mediator Transport

Figure 4.12 summarizes the two sections above. The line representing $k = 50$ [1/s] is flat until a flow speed of around 0.4 [m/s], meaning that an increase in the mass transfer coefficient does not yield an increase in the mass transfer corresponding to equation 4.6. The same holds for the first parts of the lines representing the rate constants 10 and 20 [1/s]. However, this flat part is not present in the line presenting $k = 1$, here the line is leveling off at higher flow rates, indicating saturation of oxidized mediator in the bulk as predicted in section 4.3.4. One can conclude that when the catalytic performance is high, speeding up the flow would lead to only a little gain in conversion, when only considering the mediator as limiting. Therefore, it will lead to higher pumping losses and thus a lesser efficiency. When $0 < \text{Ha} < 2$, optimizing depends on the trade-off between pumping losses and overpotential reduction.

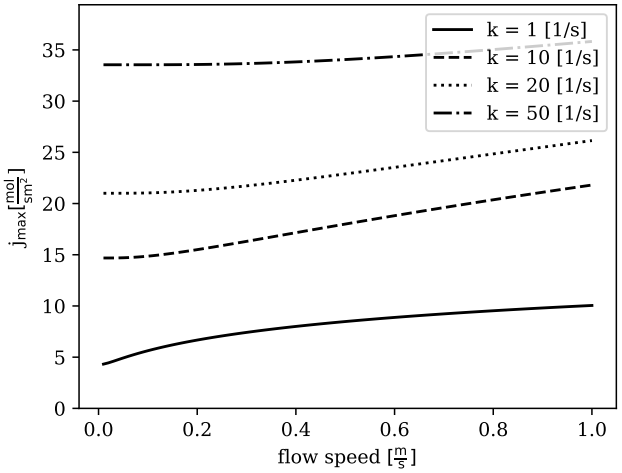

Figure 4.12: Mediators with different rate constants show that if the rate goes up, the marginal increase with flow speed gets reduced. Equation 4.7 was used, with the following parameters: $\varepsilon = 0.95$, a_v = 5400 [1/m] and D=5 10^{-10} [m^2/s].

4.4. Buffer Depletion at the Membrane

When only considering the mediator, with high catalytic activity, increasing the flow speed will not benefit the efficiency of the reactor. However, if the flow would come to a hold, other issues will arise. As explained in section 2.3.4 a buffer limitation towards the membrane could cause limitations. The limiting current inflicted by the buffer is dependent on the flow velocity. The maximum current density given by the buffer on a 10x10 cm laboratory cell is given in Figure 4.13

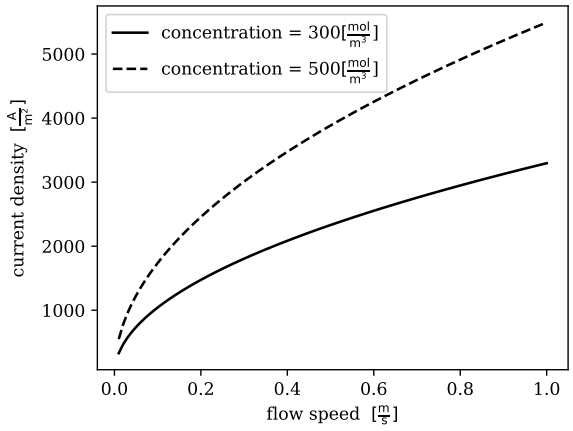

Figure 4.13: Current density sustainable by the buffer vs flow speed. The buffer concentration is the concentration of the buffer species that is actually taking on the hydroxide ions. With the following properties used: $\varepsilon = 0.95$, a_v = 5400 [1/m] and D_{buffer} = 1.4 10^{-9} [m^2/s].

However, essential to note here is that when considering dispersion, the limiting buffer current will dramatically increase. Although axial dispersion correlations exist [32], they are meant for the dispersion in the porous medium, but not dispersion to the wall.

5

Conclusion and Recommendations

5.1. Conclusion

This research aimed at optimizing the anode-side of a continuous-flow-through reactor, hosting the production of chemicals by mediated electrochemical oxidation, using organic aminoxyls (i.e., electrocatalysts), more specifically 2,2,6,6-tetramethylpiperidinyloxyl (TEMPO) and 4-acetamido-TEMPO (ACT).

An extensive literature review was carried out to identify the requirements of the reactor and the chemical characteristics of organic aminoxyl mediators that are determining for the speed of the conversion. It was found that, first of all, for TEMPO to be stable, the pH should be maintained between 7.3 and 14 and for ACT between 6.4 and 11.8. Secondly, the aminoxyls were found to be reversible and finally, an attempt was made into finding the rate constants of TEMPO and ACT with PDO, yielding a rate constant of 1.9 and 5.5 [1/s] respectfully.
Building on the literature review, a 2D COMSOL model was created featuring the reactions kinetics, hydrodynamics and current distribution. One of the main results obtained from the model is that the concentration of the oxidized mediator does not change over the length of the reactor. Instead, a reaction layer would form next to the membrane and expand into the anode with increasing current density. This suggests that the model can be simplified.

This simplification expressed itself in an analytical formula, equation 3.20, that was validated with the 2D model. The formula and the model are in good agreement over the whole domain. In order the make the model more practically relevant, mass transfer between the surface and the bulk was added, resulting in equation 3.23. A general optimization was difficult, nevertheless some conclusions can be drawn. First of all, it can be said that increasing the concentration of the mediators and electrolyte conductivity has a significant impact on the reactor's efficiency. Second of all, the formula showed that for every current there is an optimal flow velocity. Thirdly, when the volumetric surface area is independent of the porosity, increasing the volumetric surface area will always yield a better reactor efficiency. Fourth, the electrode thickness does not influence the electrochemistry, yet it does influence the pumping losses. Moreover, although the thickness does not influence the electrochemistry, the electrochemistry does determine the minimal electrode thickness required. Finally, when a mediator is very catalytically active, resulting in a Hatta number higher than 2, (Ha > 2), increasing the flow unit Ha = 2 will not contribute to a higher achievable current density. When the Hatta number is lower than 2, (0 > Ha > 2), the flow speed does influence the highest achievable current, resulting in a trade-off between pumping losses and overpotential reduction.

5.2. Recommendations

5.2.1. General

Economical Evaluation

An economical evaluation of the entire conversion process could provide more insight into the most profitable conditions for the reactor, making the model more practically applicable. From Figure 4.9, it stands out that when the current density increases, the efficiency decreases. Therefore, the optimal operating conditions are dictated by economics. Moreover, in an economical evaluation, the separation process that takes place after the reactor should also be taken into account to find the most profitable conditions for the whole process. For instance, increasing the mediator concentration in the electrolyte would yield a higher reactor efficiency. However, if this makes the separation process more difficult afterward, it is rather costly and thus not profitable. All in all, economically motivated research yields key insights into the viability of commercialization of the process.

Consider other Porous Media

In this research, only nickel, metal foams were considered as porous electrode material in the reactor. By adapting the friction factor and the Sherwood correlation, it would allow one to investigate other porous electrode structures as well, such as carbon felts and paper. It would be interesting to analyze whether these materials yield higher efficiency.

5.2.2. Experimental

Experimental Validation

Both the analytical- as well as the computational model presented in this research provide the same results, despite the fact that they were modeled differently. Although these models definitely provided fruitful insights, their credibility could be further established by experimental validation.

More Experiments on the Chemical Rate Constants between Mediator and Substrate

Further research is needed to find a way to extract the rate constants of the oxidation of PDO, by TEMPO. This research attempted to do so, as shown in appendix A. However, the results are not considered reliable because of their lack of coherence. Most literature reviewed, revolved around cyclic voltammograms (CV) or rotating disk experiments (RDE) as means to extract rate constants. These experiments however, may not be adequate tools to use, since the mediator changes from TEMPO to $TEMPO^+$ to TEMPOH. This means that if a reactor would run for some time, TEMPO would only exist temporarily at the electrode surface, and the bulk would consist of $TEMPO^+$ and TEMPOH. This transformation is not captured by CV's of RDE's, making them inaccurate. Nevertheless, these constants are needed in order to validate the analytical model. If an adequate method were to be found to retrieve the rate constants, multiple chemistries could be tested and used together with the analytical solution of this report to estimate the reactor's performance when utilized.

5.2.3. Modeling

Extend the Model

This research modelled an electrochemical and a coupled chemical reaction. Nevertheless, there are numerous of other variations of this combination. For instance, after the oxidation of PDO to LA, the oxidation continues at a lower rate towards pyvuric acid. Modelling the latter reaction would be an interesting addition to this research, because it would contribute to the further optimization of the reactor.

Dispersion

In this research, dispersion was not modelled. Dispersion is additional mass transfer induced by microscopic effects in porous media. Often it is simulated by an artificial diffusion coefficient. In this research's simulations, the buffer suffered depletion at the membrane. However, in reality this may not happen due to the effect of dispersion. Experiments are therefore needed to show there is more mass transfer than predicted by equation 2.27.

Flow by Model

From an economical point of view it would be interesting to know the achievable current densities and accompanied efficiencies of a flow-by configuration. The findings of this report form the ideal basis to establish such a model capable of determining these particulars.

Appendix A

A.1. Experimental: cyclic voltammetry measurements

The electrolyte used was a buffer of 0.5M boric acid (BA) at a pH of 9.2. Two different mediators were used, TEMPO and 4-acetamido-TEMPO (ACT). The pH of the BA buffer was adjusted by adding 1M of NaOH till the desired pH was reached. As working electrode (WE) a graphite rod of surface area of 1 cm2 was used, shown in Figure 3 and as counter electrode (CE) a coiled platinum wire was used. The reference electrode (RE) was a Ag/AlCl. Nitrogen gas was bubbled through the solution and the solution was vigorously stirred. The equipment was set up as shown in Figure A.1. The electrodes were connected to the potentiostat, which applied potential scans at 10, 20, 50 and 100 mV/s. First the potential was increased with the selected scan rate and then decreased with the same rate to create a cyclic voltammetry (CV) and during this procedure the current is constantly measured.

For the experiments the following setup was used, in Figure A.1: Varied electrolyte compositions

Figure A.1: Experimental setup with with the single compartmetn electrochemical cell, the working electrode indicated as WE, the reference electrode as RE and the counter electrode as CE; electrolyte buffer of 0.5M boric acid at a pH of 9.2.

used during the CV measurements are provided in Table A.1 For every different electrolyte composition, 4 scans with different scan rates were performed. For the test with substrate a concentration of 140 mM of PDO was chosen. In previous tests performed by TNO it was shown that increasing the concentration further than 100 mM did not have any effect on the current density.

Measurement number	Electrolyte composition
1	7.5mM TEMPO
2	7.5mM TEMPO + 140mM PDO
3	15mM TEMPO
4	15mM TEMPO + 140mM PDO
5	7.5mM ACT
6	7.5mM ACT + 140mM PDO
7	15mM ACT
8	15mM ACT + 140mM PDO

Table A.1: Table with the executed experiments, the electrolyte in all experiments contained a 0.5M boric acid buffer.

A.2. Analysis of cyclic voltammetry results

The analysis performed was found in works by Lee [37], however it was first introduced by Saveant [51]. To find the the peak current of a CV the Randles–Sevcik equation A.1 can be used.

$$i_p = 0.4463 n' F A c_{0,\text{med}} \sqrt{\frac{n' F \nu D}{RT}}, \tag{A.1}$$

where ν is the scan rate in [V/s], i_p is the peak current [A/m^2] and n' is the amount of electrons needed for the mediator in absence of the substrate, here it is two since the mediator transports 2 electrons from propandiol. The plateau current of the catalyst combined with the substrate is given by equation A.2 [51]:

$$i_{\text{pl}} = nFAc_{0,\text{med}} \sqrt{Dk_{obs}}, \tag{A.2}$$

where k_obs is the first order observed rate constant in [1/s]. By dividing the plateau current, equation A.2, by the peak current, equation A.1, equation A.3 is obtained:

$$\frac{i_{\text{pl}}}{i_p} = \frac{n}{0.4463 n'} \sqrt{\frac{RTk_{obs}}{n' F \nu}}, \tag{A.3}$$

here conveniently, the electrode area and the mediator concentration drop out, leaving only the first order rate constant as a unknown. Important here is that the rate is both the same rate and concentration needs to be used.

A.3. Experimental Results

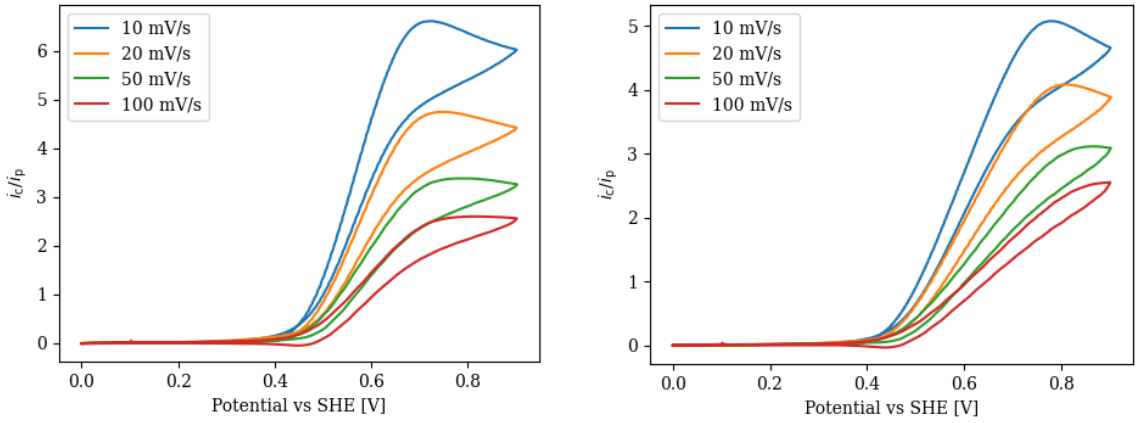

(a) 7.5 mmol of TEMPO

(b) 15 mmol of TEMPO

Figure A.2: Plots where the current of the CV with 140mM PDO and TEMPO is divided by the peak current of the TEMPO.

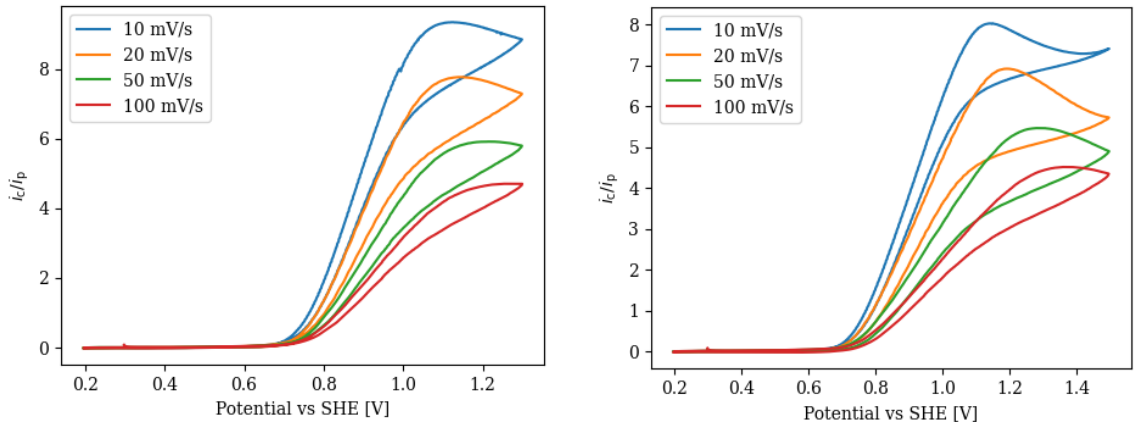

(a) 7.5 mmol of ACT

(b) 15 mmol of ACT

Figure A.3: Plots where the current of the CV with 140mM PDO and ACT is divided by the peak current of the ACT.

A.4. Determined rate constants

The obtained results show that the calculated rate constant is dependent on the scan rate, shown in Figure A.4. This implies that the rates obtain should be used with caution. Though the can still serve as a rough estimate.

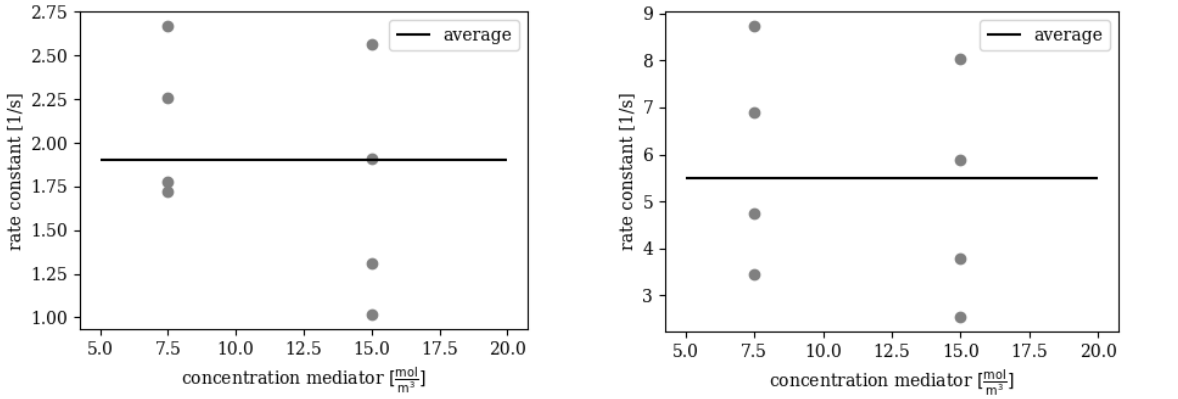

(a) The rate constant obtained for TEMPO, it is average 1.90, a maximum of 2.67 and a minimum of 1.01 [1/s]

(b) The rate constant obtained for ACT, it is average 5.50, a maximum of 8.73 and a minimum of 2.54 [1/s]

Figure A.4: A plot of the rate constants of both TEMPO and ACT combined with 140mM PDO

Bibliography

[1] Data sheet nickel foam. URL http://www.metalfoam.nl/wp-content/uploads/2019/04/datasheet_nickel.pdf.

[2] *Electrochemistry Module User's Guide*. COMSOL Multiphysics® v. 5.4. COMSOL AB, 2018. URL https://doc.comsol.com/5.4/doc/com.comsol.help.echem/ElectrochemistryModuleUsersGuide.pdf.

[3] *Subsurface Flow Module User's Guide*. COMSOL Multiphysics® v. 5.4. COMSOL AB, 2018. URL https://doc.comsol.com/5.4/doc/com.comsol.help.ssf/SubsurfaceFlowModuleUsersGuide.pdf.

[4] A. Aguirre, V. Chandra, E.A.J.F. Peters, J.A.M. Kuipers, and M.F. Open-cell foams as catalysts support: A systematic analysis of the mass transfer limitations. *Chemical Engineering Journal*, 393:124656, 2020. ISSN 1385-8947. doi: https://doi.org/10.1016/j.cej.2020.124656. URL http://www.sciencedirect.com/science/article/pii/S1385894720306471.

[5] A.J. Bard and L.R. Faulkner. *Electrochemical Methods: Fundamentals and Applications*. Wiley, 2000. ISBN 9780471043720. URL https://books.google.nl/books?id=kv56QgAACAAJ.

[6] Martin Bazant. Lecture 29: Forced convection ii, Spring 2014. URL https://ocw.mit.edu/courses/chemical-engineering/10-626-electrochemical-energy-systems-spring-2014/lecture-notes/MIT10_626S14_Lec29.pdf.

[7] Jacob Bear. *Fundamental Balance Equations and Fluxes*, pages 175–254. Springer International Publishing, Cham, 2018. ISBN 978-3-319-72826-1. doi: 10.1007/978-3-319-72826-1_3. URL https://doi.org/10.1007/978-3-319-72826-1_3.

[8] R.B. Bird, W.E. Stewart, and E.N. Lightfoot. *Transport Phenomena*. Wiley International edition. Wiley, 2006. ISBN 9780470115398. URL https://books.google.nl/books?id=L5FnNlIaGfcC.

[9] K. Boomsma, D. Poulikakos, and Y. Ventikos. Simulations of flow through open cell metal foams using an idealized periodic cell structure. *International Journal of Heat and Fluid Flow*, 24(6):825 – 834, 2003. ISSN 0142-727X. doi: https://doi.org/10.1016/j.ijheatfluidflow.2003.08.002. URL http://www.sciencedirect.com/science/article/pii/S0142727X03001103.

[10] Mauro Bracconi, Matteo Ambrosetti, Matteo Maestri, Gianpiero Groppi, and Enrico Tronconi. A fundamental investigation of gas/solid mass transfer in open-cell foams using a combined experimental and cfd approach. *Chemical Engineering Journal*, 352:558 – 571, 2018. ISSN 1385-8947. doi: https://doi.org/10.1016/j.cej.2018.07.023. URL http://www.sciencedirect.com/science/article/pii/S1385894718312506.

[11] David J. Chadderdon, Le Xin, Ji Qi, Brian Brady, Julie A. Miller, Kai Sun, Michael J. Janik, and Wenzhen Li. Selective oxidation of 1,2-propanediol in alkaline anion-exchange membrane electrocatalytic flow reactors: Experimental and dft investigations. *ACS Catalysis*, 5(11):6926–6936, 2015. doi: 10.1021/acscatal.5b01085. URL https://doi.org/10.1021/acscatal.5b01085.

[12] Cyrille Costentin and Jean-Michel Savéant. Multielectron, multistep molecular catalysis of electrochemical reactions: Benchmarking of homogeneous catalysts. *ChemElectroChem*, 1(7):1226–1236, 2014. doi: 10.1002/celc.201300263. URL https://chemistry-europe.onlinelibrary.wiley.com/doi/abs/10.1002/celc.201300263.

[13] F. G. Cuevas, J. M. Montes, J. Cintas, and P. Urban. Electrical conductivity and porosity relationship in metal foams. *Journal of Porous Materials*, 16(6):675–681, 2009. doi: 10.1007/s10934-008-9248-1.

[14] Peter V Danckwerts. Continuous flow systems: distribution of residence times. *Chemical engineering science*, 2(1):1–13, 1953.

[15] Saurish Das, Niels G. Deen, and J. A. M. Kuipers. Immersed boundary method (ibm) based direct numerical simulation of open-cell solid foams: Hydrodynamics. *AIChE Journal*, 63(3):1152–1173, 2017. doi: 10.1002/aic.15487. URL https://aiche.onlinelibrary.wiley.com/doi/abs/10.1002/aic.15487.

[16] Bruno Delille. Co2 in seawater: Equilibrium, kinetics, isotopes richard e. zeebe and dieter wolf-gladrow, elsevier oceanography series 65, amsterdam, 2001, (paperback) isbn: 0444509461. *Journal of Marine Systems - J MARINE SYST*, 36:269–270, 01 2002.

[17] Benjamin Dietrich. Pressure drop correlation for ceramic and metal sponges. *Chemical Engineering Science*, 74:192 – 199, 2012. ISSN 0009-2509. doi: https://doi.org/10.1016/j.ces.2012.02.047. URL http://www.sciencedirect.com/science/article/pii/S0009250912001431.

[18] Nikolaos Dimitratos, Jose Antonio Lopez-Sanchez, Sankar Meenakshisundaram, Jinto Manjaly Anthonykutty, Gemma Brett, Albert F. Carley, Stuart H. Taylor, David W. Knight, and Graham J. Hutchings. Selective formation of lactate by oxidation of 1,2-propanediol using gold palladium alloy supported nanocrystals. *Green Chem.*, 11:1209–1216, 2009. doi: 10.1039/B823285G. URL http://dx.doi.org/10.1039/B823285G.

[19] T.Q.N. Do, M. Varničić, R.J. Flassig, T. Vidaković-Koch, and K. Sundmacher. Dynamic and steady state 1-d model of mediated electron transfer in a porous enzymatic electrode. *Bioelectrochemistry*, 106:3 – 13, 2015. ISSN 1567-5394. doi: https://doi.org/10.1016/j.bioelechem.2015.07.007. URL http://www.sciencedirect.com/science/article/pii/S1567539415300128.

[20] Fengmin Du, David M. Warsinger, Tamanna I. Urmi, Gregory P. Thiel, Amit Kumar, and John H. Lienhard V. Sodium hydroxide production from seawater desalination brine: Process design and energy efficiency. *Environmental Science & Technology*, 52(10):5949–5958, 2018. doi: 10.1021/acs.est.8b01195. URL https://doi.org/10.1021/acs.est.8b01195. PMID: 29669210.

[21] N. Dukhan. *Metal Foams: Fundamentals and Applications*. DEStech Publications, Incorporated, 2013. ISBN 9781605950143. URL https://books.google.nl/books?id=xZRG1EyBbzsC.

[22] Noémie Elgrishi, Kelley J. Rountree, Brian D. McCarthy, Eric S. Rountree, Thomas T. Eisenhart, and Jillian L. Dempsey. A practical beginner's guide to cyclic voltammetry. *Journal of Chemical Education*, 95(2):197–206, 2018. doi: 10.1021/acs.jchemed.7b00361. URL https://doi.org/10.1021/acs.jchemed.7b00361.

[23] Judith R. Fish, Steven G. Swarts, Michael D. Sevilla, and Tadeusz Malinski. Electrochemistry and spectroelectrochemistry of nitroxyl free radicals. *The Journal of Physical Chemistry*, 92(13):3745–3751, 1988. doi: 10.1021/j100324a012. URL https://doi.org/10.1021/j100324a012.

[24] James B. Gerken, Yutong Q. Pang, Markus B. Lauber, and Shannon S. Stahl. Structural effects on the ph-dependent redox properties of organic nitroxyls: Pourbaix diagrams for tempo, abno, and three tempo analogs. *The Journal of Organic Chemistry*, 83(14):7323–7330, 2018. doi: 10.1021/acs.joc.7b02547. URL https://doi.org/10.1021/acs.joc.7b02547. PMID: 29182282.

[25] Nicolas Glandut, Andrew Malec, Michael Mirkin, and Marcin Majda. Electrochemical studies of the lateral diffusion of tempo in the aqueous liquid/vapor interfacial region. *The journal of physical chemistry. B*, 110:6101–9, 04 2006. doi: 10.1021/jp0570824.

[26] Russell Goodall, Ludger Weber, and Andreas Mortensen. The electrical conductivity of microcellular metals. *Journal of Applied Physics*, 100(4):044912, 2006. doi: 10.1063/1.2335672. URL https://doi.org/10.1063/1.2335672.

[27] S. Hatta. On the absorption velocity of gases by liquids-ii: Theoretical considerations of gas absorption due to chemical reaction. *Technological Reports of Tôhoku University*, 10:613–622, 1932.

[28] J.W. Haverkort. personal communication.

[29] J.W. Haverkort. A theoretical analysis of the optimal electrode thickness and porosity. *Electrochimica Acta*, 295:846 – 860, 2019. ISSN 0013-4686. doi: https://doi.org/10.1016/j.electacta.2018.10.065. URL http://www.sciencedirect.com/science/article/pii/S0013468618323041.

[30] David P. Hickey, Matthew S. McCammant, Fabien Giroud, Matthew S. Sigman, and Shelley D. Minteer. Hybrid enzymatic and organic electrocatalytic cascade for the complete oxidation of glycerol. *Journal of the American Chemical Society*, 136(45):15917–15920, 2014. doi: 10.1021/ja5098379. URL https://doi.org/10.1021/ja5098379. PMID: 25350383.

[31] David P. Hickey, David A. Schiedler, Ivana Matanovic, Phuong Vy Doan, Plamen Atanassov, Shelley D. Minteer, and Matthew S. Sigman. Predicting electrocatalytic properties: Modeling structure–activity relationships of nitroxyl radicals. *Journal of the American Chemical Society*, 137 (51):16179–16186, 2015. doi: 10.1021/jacs.5b11252. URL https://doi.org/10.1021/jacs.5b11252. PMID: 26635089.

[32] C. Hutter, A. Zenklusen, R. Lang, and Ph. Rudolf von Rohr. Axial dispersion in metal foams and streamwise-periodic porous media. *Chemical Engineering Science*, 66(6):1132 – 1141, 2011. ISSN 0009-2509. doi: https://doi.org/10.1016/j.ces.2010.12.016. URL http://www.sciencedirect.com/science/article/pii/S0009250910007293.

[33] Avner Israeli, Miriam Patt, Miriam Oron, Amram Samuni, Ron Kohen, and Sara Goldstein. Kinetics and mechanism of the comproportionation reaction between oxoammonium cation and hydroxylamine derived from cyclic nitroxides. *Free Radical Biology and Medicine*, 38(3):317 – 324, 2005. ISSN 0891-5849. doi: https://doi.org/10.1016/j.freeradbiomed.2004.09.037. URL http://www.sciencedirect.com/science/article/pii/S0891584904008329.

[34] Maria Janiszewska, Grzeszczuk. Mechanistic – kinetic scheme of oxidation/reduction of tempo involving hydrogen bonded dimer. rde probe for availability of protons in reaction environment. *Electroanalysis*, 16(20):1673–1681, 2004. doi: 10.1002/elan.200303011. URL https://onlinelibrary.wiley.com/doi/abs/10.1002/elan.200303011.

[35] Lida Khalafi and Mohammad Rafiee. *Cyclic Voltammetry*, pages 1–42. American Cancer Society, 2017. ISBN 9781118468586. doi: 10.1002/9781118468586.epoc4036. URL https://onlinelibrary.wiley.com/doi/abs/10.1002/9781118468586.epoc4036.

[36] Lori E. Koelsch. Reconceptualizing the member check interview. *International Journal of Qualitative Methods*, 12(1):168–179, 2013. doi: 10.1177/160940691301200105. URL https://doi.org/10.1177/160940691301200105.

[37] Katherine Lee, Noémie Elgrishi, Banu Kandemir, and Jillian Dempsey. Electrochemical and spectroscopic methods for evaluating molecular electrocatalysts. *Nature Reviews Chemistry*, 1, 05 2017. doi: 10.1038/s41570-017-0039.

[38] Katherine J. Lee, Cole T. Gruninger, Kunal M. Lodaya, Saad Qadeer, Boyce E. Griffith, and Jillian L. Dempsey. Analysis of multi-electron, multi-step homogeneous catalysis by rotating disc electrode voltammetry: theory, application, and obstacles. *Analyst*, 145:1258–1278, 2020. doi: 10.1039/C9AN02192B. URL http://dx.doi.org/10.1039/C9AN02192B.

[39] Robert Lemlich. A theory for the limiting conductivity of polyhedral foam at low density. *Journal of Colloid and Interface Science*, 64(1):107 – 110, 1978. ISSN 0021-9797. doi: https://doi.org/10.1016/0021-9797(78)90339-9. URL http://www.sciencedirect.com/science/article/pii/0021979778903399.

[40] O. Levenspiel and Knovel (Firm). *Chemical Reaction Engineering*. Wiley, 1999. ISBN 9780471254249. URL https://books.google.hu/books?id=X4svAQAAIAAJ.

[41] James Lunt. Large-scale production, properties and commercial applications of polylactic acid polymers. *Polymer Degradation and Stability*, 59(1):145 – 152, 1998. ISSN 0141-3910. doi: https://doi.org/10.1016/S0141-3910(97)00148-1. URL http://www.sciencedirect.com/science/article/pii/S0141391097001481. Biodegradable Polymers and Macromolecules.

[42] Youssef Naimi and Amal Antar. Hydrogen generation by water electrolysis. In Murat Eyvaz, editor, *Advances In Hydrogen Generation Technologies*, chapter 1. IntechOpen, Rijeka, 2018. doi: 10.5772/intechopen.76814. URL https://doi.org/10.5772/intechopen.76814.

[43] J. Newman and K.E. Thomas-Alyea. *Electrochemical Systems*. The ECS Series of Texts and Monographs. Wiley, 2004. ISBN 9780471477563. URL https://books.google.nl/books?id=vArZu0HM-xYC.

[44] R. S. Nicholson and Irving. Shain. Theory of stationary electrode polarography. single scan and cyclic methods applied to reversible, irreversible, and kinetic systems. *Analytical Chemistry*, 36(4):706–723, 1964. doi: 10.1021/ac60210a007. URL https://doi.org/10.1021/ac60210a007.

[45] Jordan E. Nutting, Mohammad Rafiee, and Shannon S. Stahl. Tetramethylpiperidine n-oxyl (tempo), phthalimide n-oxyl (pino), and related n-oxyl species: Electrochemical properties and their use in electrocatalytic reactions. *Chemical Reviews*, 118(9):4834–4885, 2018. doi: 10.1021/acs.chemrev.7b00763. URL https://doi.org/10.1021/acs.chemrev.7b00763. PMID: 29707945.

[46] Elena Pérez-Gallent, Susan Turk, Roman Latsuzbaia, Rajat Bhardwaj, Anca Anastasopol, Francesc Sastre-Calabuig, Amanda Cristina Garcia, Erwin Giling, and Earl Goetheer. Electroreduction of co2 to co paired with 1,2-propanediol oxidation to lactic acid. toward an economically feasible system. *Industrial & Engineering Chemistry Research*, 58(16):6195–6202, 2019. doi: 10.1021/acs.iecr.8b06340. URL https://doi.org/10.1021/acs.iecr.8b06340.

[47] Elena Pérez-Gallent, Carlos Sánchez-Martínez, Leon F. G. Geers, Susan Turk, Roman Latsuzbaia, and Earl L. V. Goetheer. Overcoming mass transport limitations in electrochemical reactors with a pulsating flow electrolyzer. *Industrial & Engineering Chemistry Research*, 59 (13):5648–5656, 2020. doi: 10.1021/acs.iecr.9b06925. URL https://doi.org/10.1021/acs.iecr.9b06925.

[48] Mohammad Rafiee, Babak Karimi, and Saber Alizadeh. Mechanistic study of the electrocatalytic oxidation of alcohols by tempo and nhpi. *ChemElectroChem*, 1(2):455–462, 2014. doi: 10.1002/celc.201300016. URL https://onlinelibrary.wiley.com/doi/abs/10.1002/celc.201300016.

[49] Mohammad Rafiee, Kelsey C. Miles, and Shannon S. Stahl. Electrocatalytic alcohol oxidation with tempo and bicyclic nitroxyl derivatives: Driving force trumps steric effects. *Journal of the American Chemical Society*, 137(46):14751–14757, 2015. doi: 10.1021/jacs.5b09672. URL https://doi.org/10.1021/jacs.5b09672. PMID: 26505317.

[50] Mohammad Rafiee, Zachary M. Konz, Matthew D. Graaf, Hannes F. Koolman, and Shannon S. Stahl. Electrochemical oxidation of alcohols and aldehydes to carboxylic acids catalyzed by 4-acetamido-tempo: An alternative to “anelli” and “pinnick” oxidations. *ACS Catalysis*, 8(7):6738–6744, 2018. doi: 10.1021/acscatal.8b01640. URL https://doi.org/10.1021/acscatal.8b01640.

[51] J.M. Saveant and E. Vianello. Potential-sweep chronoamperometry: Kinetic currents for first-order chemical reaction parallel to electron-transfer process (catalytic currents). *Electrochimica Acta*, 10(9):905 – 920, 1965. ISSN 0013-4686. doi: https://doi.org/10.1016/0013-4686(65)80003-2. URL http://www.sciencedirect.com/science/article/pii/0013468665800032.

[52] K. Scott and A. N. Haines. Mathematical reactor modelling for coupled chemical and electrochemical processes: the ece system. *Journal of Applied Electrochemistry*, 24(8):703–712, Aug 1994. ISSN 1572-8838. doi: 10.1007/BF00578083. URL https://doi.org/10.1007/BF00578083.

[53] A.A. Shah, M.J. Watt-Smith, and F.C. Walsh. A dynamic performance model for redox-flow batteries involving soluble species. *Electrochimica Acta*, 53(27):8087 – 8100, 2008. ISSN 0013-4686. doi: https://doi.org/10.1016/j.electacta.2008.05.067. URL http://www.sciencedirect.com/science/article/pii/S0013468608007214.

[54] E. W. Thiele. Relation between catalytic activity and size of particle. *Industrial & Engineering Chemistry*, 31(7):916–920, 1939. doi: 10.1021/ie50355a027. URL https://doi.org/10.1021/ie50355a027.

[55] M. Tsunaga, C. Iwakura, and H. Tamura. Electrode reactions of nitroxide radicals at platinum in acetonitrile. *Electrochimica Acta*, 18(3):241 – 245, 1973. ISSN 0013-4686. doi: https://doi.org/10.1016/0013-4686(73)80020-9. URL http://www.sciencedirect.com/science/article/pii/0013468673800209.

[56] E.P. van Elk, P.C. Borman, J.A.M. Kuipers, and G.F. Versteeg. Modelling of gas–liquid reactors — implementation of the penetration model in dynamic modelling of gas–liquid processes with the presence of a liquid bulk. *Chemical Engineering Journal*, 76(3):223 – 237, 2000. ISSN 1385-8947. doi: https://doi.org/10.1016/S1385-8947(99)00162-X. URL http://www.sciencedirect.com/science/article/pii/S138589479900162X.

[57] W.P.M. van Swaaij and G.F. Versteeg. Mass transfer accompanied with complex reversible chemical reactions in gas—liquid systems: an overview. *Chemical Engineering Science*, 47(13):3181 – 3195, 1992. ISSN 0009-2509. doi: https://doi.org/10.1016/0009-2509(92)85028-A. URL http://www.sciencedirect.com/science/article/pii/000925099285028A.

[58] Ming-Hung Wang, Allan N. Soriano, Alvin R. Caparanga, and Meng-Hui Li. Binary mutual diffusion coefficient of aqueous solutions of propylene glycol and dipropylene glycol. *Journal of the Taiwan Institute of Chemical Engineers*, 41(3):279 – 285, 2010. ISSN 1876-1070. doi: https://doi.org/10.1016/j.jtice.2009.09.001. URL http://www.sciencedirect.com/science/article/pii/S1876107009001382.

[59] Robert C Weast, 1928 Lide, David R., and University of Rhode Island. Coastal Resources Center. Crc handbook of chemistry and physics. 1978. ISSN 0147-6262. URL http://bibpurl.oclc.org/web/11915. "A ready-reference book of chemical and physical data.".

[60] A.C. West. *Electrochemistry and Electrochemical Engineering: An Introduction*. Alan C. West, 2012. ISBN 9781470076047.